Canadian Mineralogist
Vol. 30, pp. 811-833 (1992)

GEOCHEMISTRY OF A BORON-RICH PERALUMINOUS GRANITE PLUTON: THE CALAMITY PEAK LAYERED GRANITE–PEGMATITE COMPLEX, BLACK HILLS, SOUTH DAKOTA

EDWARD F. DUKE

Engineering and Mining Experiment Station and Department of Geology and Geological Engineering, South Dakota School of Mines and Technology, Rapid City, South Dakota 57701-3995, U.S.A.

JAMES J. PAPIKE

Institute of Meteoritics and Department of Geology, University of New Mexico, Albuquerque, New Mexico 87131, U.S.A.

JAGDISH C. LAUL

Chemical Technology Division, Battelle Pacific Northwest Laboratories, Richland, Washington 99352, U.S.A.

ABSTRACT

The Calamity Peak pluton is a small, layered granite–pegmatite intrusive body associated with the Harney Peak Granite in the Black Hills, South Dakota. The pluton is texturally and chemically heterogeneous; it consists predominantly of tourmaline – muscovite – garnet granite and pegmatite, along with minor muscovite – biotite – garnet granite, and includes approximately 400 m of alternating granite and pegmatite, in layers 0.1–2.0 m thick. Pegmatite layers are enriched in perthite whereas granite layers contain relatively more albite and tourmaline so that $Na_2O/(Na_2O+K_2O)$ ranges from 0.37 to 0.91. Along with Na, granite layers are relatively enriched in B, Mg, Ca, Fe, Zn, Zr, *REE*, Hf, Th, and U, whereas pegmatite layers are relatively enriched in K, As, Rb, Nb, Cs, Ba, Ta, and Pb, and have higher Eu/Eu^*. Relative to "primitive" biotite granites that occur in other portions of the Harney Peak Granite, rocks at Calamity Peak are enriched in B (~5× – 80×), Na, P, Mn, As, Sb, Cs, and Ta, but depleted in Mg, K, Ca, Sc, Ti, Cr, Fe, Co, Cu, Sr, Y, Zr, Ba, Hf, Pb, Th, U, and all *REE* except Lu. Depletion in thorium and *LREE* is attributed to early crystallization and separation of monazite. Enrichment in Na at Calamity Peak and the development of prominent igneous layering are attributed to phase-equilibrium shifts induced by the high B content of the magmas. The overall chemical changes are consistent with derivation of the least fractionated Calamity Peak compositions through 70% fractional crystallization of Harney Peak biotite granites; this agrees with structural evidence that the Calamity Peak pluton formed after much of the main Harney Peak Granite dome had been emplaced.

Keywords: granite, pegmatite, igneous layering, peraluminous, boron, geochemistry, rare-earth elements, trace element modeling, Black Hills, South Dakota.

SOMMAIRE

Le pluton de Calamity Peak, petit massif intrusif composé de granite et de pegmatite lités, est associé au granite de Harney Peak dans la région des Black Hills (Dakota du Sud). Le pluton est hétérogène dans sa composition et ses textures. Il est fait surtout de granite et de pegmatite à tourmaline – muscovite – grenat, et contient aussi un granite à muscovite – biotite – grenat, de même qu'une séquence d'environ 400 m de granite et de pegmatite, en alternance, en couches entre 0.1 et 2 m d'épaisseur. Les niveaux pegmatitiques sont enrichis en perthite, tandis que les niveaux granitiques contiennnent plus d'albite et de tourmaline, de sorte que le rapport $Na_2O/(Na_2O+K_2O)$ varie de 0.37 à 0.91. Outre le Na, les niveaux granitiques sont plus riches en B, Mg, Ca, Fe, Zn, Zr, les terres rares, Hf, Th et U, tandis que les niveaux pegmatitiques sont plus riches en K, As, Rb, Nb, Cs, Ba, Ta et Pb; de plus, ces derniers ont un rapport Eu/Eu^* plus élevé. En comparaison des granites à biotite plus primitifs qui font partie du granite de Harney Peak, les roches de Calamity Peak sont enrichies en B (~5X –80X), Na, P, Mn, As, Sb, Cs et Ta, et appauvries en Mg, K, Ca, Sc, Ti, Cr, Fe, Co, Cu, Sr, Y, Zr, Ba, Hf, Pb, Th, U, et toutes les terres rares sauf Lu. Nous attribuons l'appauvrissement en Th et les terres rares légères à la cristallisation précoce et au fractionnement de la monazite. L'enrichissement en Na et le développement d'un litage igné seraient dus à l'effet du bore sur l'équilibre des phases dans le magma. Les changements en composition au cours du fractionnement dans ce système concordent avec l'hypothèse que le magma le moins évolué à Calamity Peak résulte d'un taux de cristallisation fractionnée de 70% du magma qui a donné le granite à biotite de Harney Peak. L'évidence structurale en faveur de la formation du pluton de Calamity Peak après la mise en place de la plupart du dome de Harney Peak étaye cette hypothèse.

(Traduit par la Rédaction)

Mots-clés: granite, pegmatite, litage igné, hyperalumineux, bore, géochimie, terres rares, modèle pétrogénétique, Black Hills, Dakota du Sud.

INTRODUCTION

The Calamity Peak granite–pegmatite complex is a small, dome-like intrusive body located approximately 2 km southwest of the much larger Harney Peak Granite dome in the southern Black Hills, South Dakota (Fig. 1). In addition to the main dome and several satellite plutons such as the one at Calamity Peak, the Harney Peak Granite includes over 20,000 individual intrusive bodies (Redden *et al.* 1982, Norton & Redden 1990). These range in composition from "normal" peraluminous granite (muscovite + biotite ± garnet) in portions of the main dome through

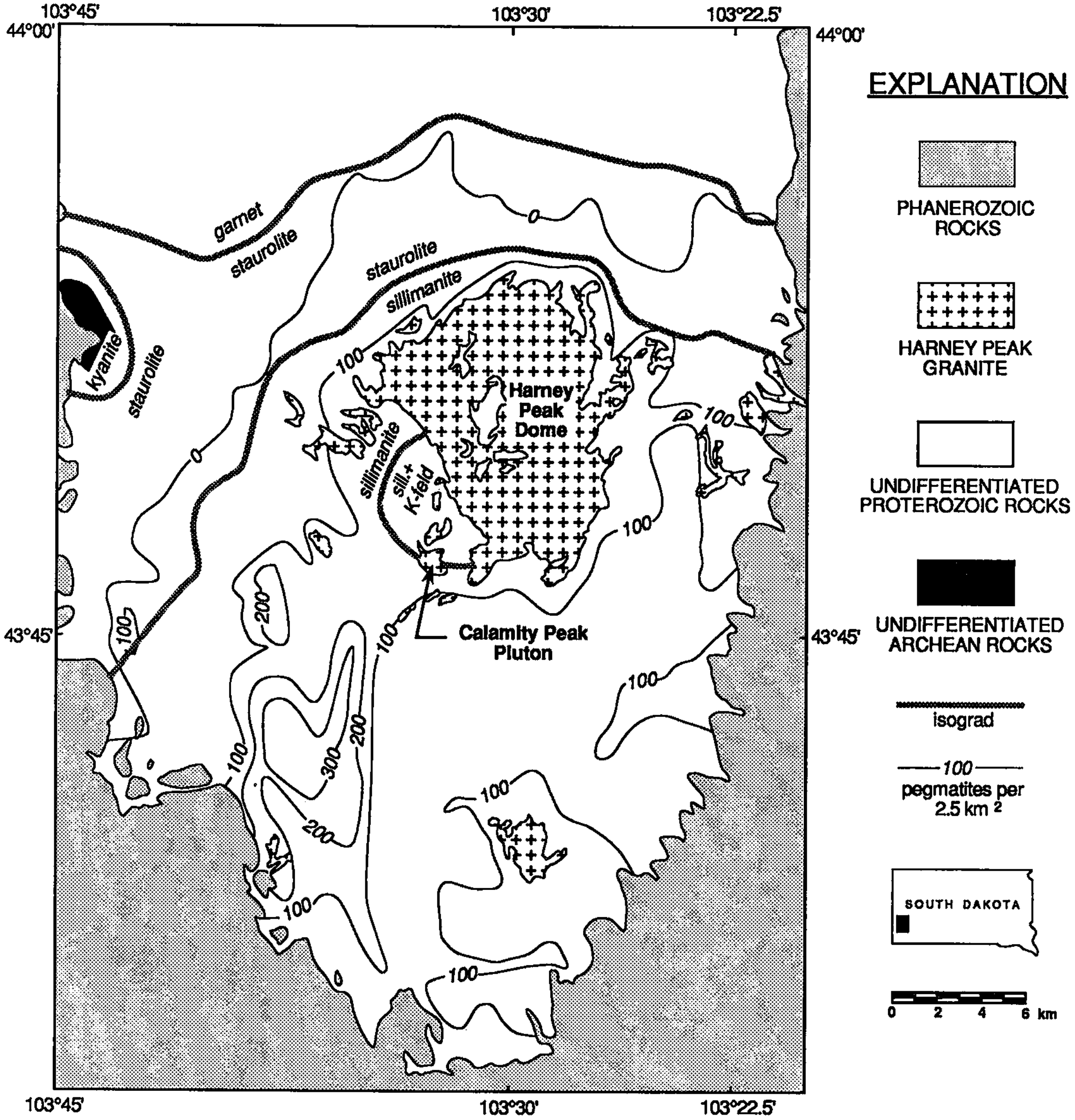

FIG. 1. Map of the southern Black Hills, showing the locations of the Calamity Peak pluton and the Harney Peak Granite dome. Also shown are the distribution of metamorphic zones and the estimated density of granitic bodies and pegmatites too small to be mapped individually on this scale. Note that 2.5 $km^2 \approx 1\ mi^2$. Modified from Redden *et al.* (1982, Fig. 1).

tourmaline-rich intrusive bodies, such as Calamity Peak, to highly evolved rare-element pegmatites (Page *et al.* 1953, Norton *et al.* 1964, Černý 1982). Černý & Meintzer (1988) cited the Harney Peak dome as a classic example of a "fertile" granite massif centrally located with respect to the surrounding pegmatite district.

In this paper, we present data on the major- and trace-element chemistry of the main rock-types in the Calamity Peak pluton, examine these results in comparison to compositions of other parts of the Harney Peak Granite, and compare the chemical data with a model for the structural evolution of the pluton. The most distinctive characteristic of the Calamity Peak pluton is its exceptionally well-developed textural and mineralogical layering, although most intrusive bodies of the Harney Peak Granite display the same layering to some extent. The development of abundant layering in the Calamity Peak pluton parallels an overall enrichment of the rocks at Calamity Peak in B and Na, compared with many portions of the main Harney Peak Granite (Rockhold *et al.* 1987, Nabelek *et al.* 1992a).

The results of this paper indicate substantial chemical variations in rocks in the Calamity Peak pluton compared with portions of the main Harney Peak Granite dome, as well as systematic differences among mapped rock units within the Calamity Peak pluton, itself. A large part of the chemical and textural heterogeneity of the pluton resulted from the pervasive effects of mineralogical segregation that accompanied crystallization. High contents of B, H_2O, and other volatiles may have promoted the development of igneous layering and other forms of mineralogical and chemical segregation. Along with the structural analysis presented by Duke *et al.* (1988), this detailed study of the geochemistry of the Calamity Peak pluton underscores the complexity of petrogenetic evolution in volatile-rich peraluminous granites, and the difficulty in defining the liquid's line-of-descent in highly evolved rocks of this suite.

REGIONAL GEOLOGICAL SETTING

Precambrian rocks of the Black Hills are dominantly metasedimentary rocks deposited between about 2.2 and 1.88 Ga; also present, however, are small exposures of Archean (~2.5 Ga) granite and older metasedimentary rocks (Gosselin *et al.* 1988, Redden *et al.* 1990). This brief summary of the Precambrian geology and tectonic evolution of the region is drawn from the detailed reviews found in DeWitt *et al.* (1986) and Redden *et al.* (1990).

The Lower Proterozoic strata consist chiefly of metamorphosed graywacke, shale, and quartzite. The main stage of Early Proterozoic regional metamorphism commenced at some time after 1.88 Ga, and major metamorphic activity ended with thermal metamorphism accompanying emplacement of the Harney Peak Granite and related rocks at 1.72 Ga. Intensity of metamorphism increased from low grade in the central Black Hills southward toward the granite, which is exposed within a broad region of sillimanite-zone metamorphism (Fig. 1). Assemblages of the sillimanite – K-feldspar zone occur in a restricted area along the southwestern flank of the Harney Peak dome in the vicinity of Calamity Peak. Metamorphic conditions in wall rocks adjacent to the Calamity Peak pluton, interpreted as conditions at the time of magma emplacement, are estimated at 600°–675°C, 3.5–5.5 kbar, on the basis of the composition of the core of minerals and thermometry and barometry on the assemblage garnet – biotite – sillimanite – plagioclase – quartz (E.F. Duke, unpubl. data).

The Early Proterozoic structural development of the Black Hills was characterized by an initial stage of north-directed nappe-like folding and thrusting along east–west or northeasterly trending axes, followed by further folding along north-northwesterly trending axes. These events were followed, in turn, by the emplacement of the Harney Peak Granite in the main domal structure, along with the development of smaller dome-like intrusive bodies, such as Calamity Peak, and the emplacement of thousands of small pegmatite and granite bodies in the adjacent rocks.

On the basis of the strongly peraluminous composition of the Harney Peak Granite, low Ca content, high $^{87}Sr/^{86}Sr_{initial}$ [0.7157: Riley (1970), recalculated by DeWitt *et al.* (1986)], high $\delta^{18}O$ (10.9–13.8‰; Walker *et al.* 1986), and low ϵ_{Nd}^{1715} (-2.0 to -9.9: Walker *et al.* 1986), it is likely that the initial granitic magmas were derived by anatexis of a sedimentary source-region. However, attempts to model the origin of various portions of the granite using compositions of exposed metasedimentary protoliths have failed to account for all the isotopic (Walker *et al.* 1986) or trace-element characteristics (Shearer *et al.* 1987) of the granite. In addition, the Nd isotope data of Walker *et al.* (1986) suggest that the protolith was at least partly Archean in age. Additional structural and chemical features of the Harney Peak Granite are described in Redden *et al.* (1982), Walker *et al.* (1986), Shearer *et al.* (1987), Duke *et al.* (1990), Redden *et al.* (1990), and Nabelek *et al.* (1992a, b).

STRUCTURE OF INTRUSIVE UNITS IN THE CALAMITY PEAK PLUTON

The structural relationships among different intrusive units of the Calamity Peak pluton were described in detail by Duke *et al.* (1988). Only those structural features that relate to rock-types analyzed for this report are reviewed here, in order to establish the proper structural context for the geochemical results discussed later. Prominent igneous layering, which occurs on several scales in the granite–pegmatite complex, is described below, as are the characteristics of discordant fracture-filling units and sills that intrude country rock adjacent to the pluton.

Meter-scale textural layers

The most conspicuous structural feature at Calamity Peak is the sequence of meter-scale textural layers that occurs throughout the pluton, reaching a thickness of approximately 400 m. Textural layering consists of alternating layers of pegmatite and equigranular granite (Fig. 2). Granite layers are, themselves, typically laminated on the millimeter scale owing to alternating laminations of light and dark minerals ("line rock"; see below). Maximum grain-size in pegmatite layers ranges from 3 cm to 1 m, whereas grain size in granite layers is generally 2 mm or less. Layers vary in thickness in different parts of the complex, but typically lie between 0.1 and 2.0 m, and persist along strike for distances of 5 to 100 m. There is considerable variation in the relative thicknesses of associated granite and pegmatite layers, but they generally occur in subequal proportions. Contacts between adjacent granite and pegmatite layers are generally sharp, but may be diffuse locally. Although the overall relationship between these layers is highly concordant, contacts of pegmatite layers may be slightly transgressive with respect to the adjacent layers of granite, and there is evidence that the material from which the pegmatite layers formed remained mobile after associated granite was largely solidified.

In terms of mineralogy, the layers of granite and pegmatite are characterized by identical assemblages of major minerals, consisting of quartz, K-feldspar (microcline perthite), plagioclase (albite), muscovite, tourmaline, and garnet, but the proportions of individual minerals vary considerably between granite and pegmatite layers. The most prominent variation is in the relative abun-

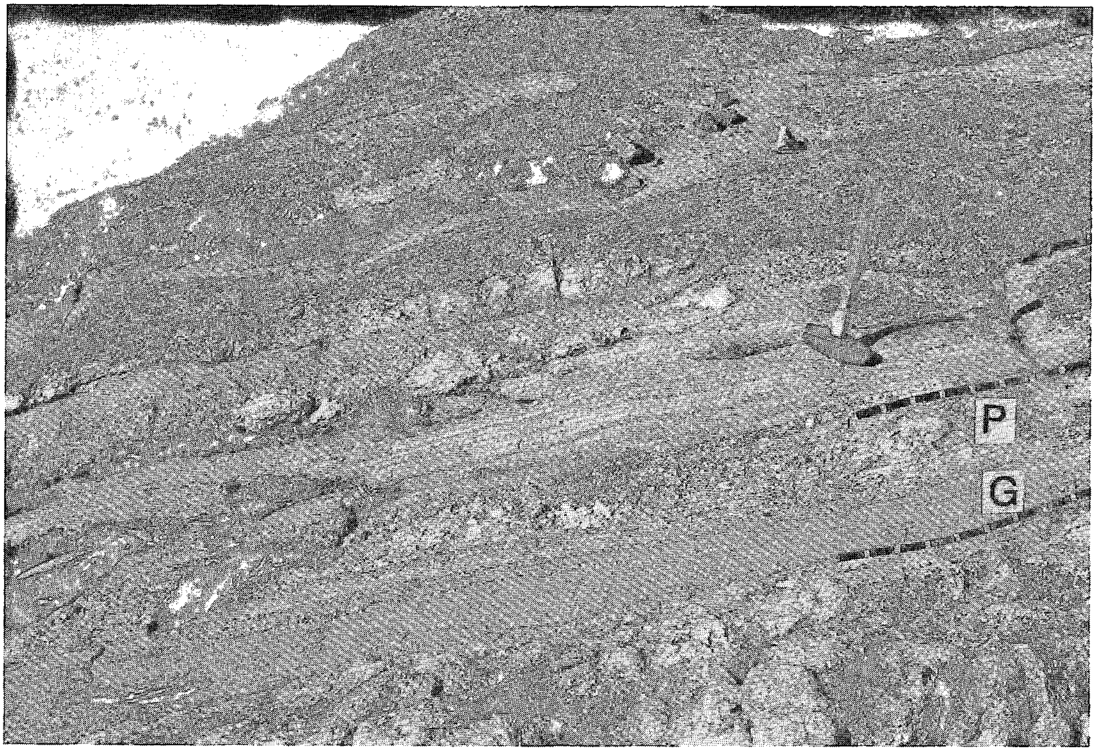

FIG. 2. Textural layering in the Calamity Peak pluton, consisting of alternating granite and pegmatite layers approximately 0.3-0.5 m thick. Granite layers exhibit millimeter-scale banding (line rock) described in text. Dashed lines on right side of photo delineate one granite–pegmatite pair: G, granite; P, pegmatite. Layers dip away from viewer at about 65°. From Duke *et al.* (1988).

dance of perthite and albite. Perthite is enriched in the pegmatite layers, and albite, in the associated granite. As an example of this tendency, Figure 5 of Duke *et al.* (1988) illustrates pegmatite layers containing 50–80 vol.% perthite in direct contact with granite layers containing less than 2 vol.% perthite. Although it amounts to 5% or less of the rock by volume, tourmaline is always more abundant in the granite layers. The other major phases are less regularly distributed; however, garnet appears to be concentrated in the granitic layers, and muscovite appears to be enriched in pegmatite layers. Accessory phases in these samples include apatite, sillimanite, graphite, arsenopyrite, monazite, beryl, and chrysoberyl; however, these occur in abundances too low to assess their distribution between the different types of layers.

In the pegmatite layers, perthite forms the largest crystals, with tourmaline, muscovite, and albite forming smaller grains that grade downward in size into a matrix of generally granitic texture. In the granite layers, there is no detectable variation in grain size between dark- and light-colored laminae in line rock. There is generally no strong preferred orientation of minerals in the line rock, either; very rarely, tourmaline is lineated parallel to the plane of the laminations. There is generally no textural indication, such as flow foliation, that the parent magma was intruded with any phenocrysts. Tourmaline (euhedral to subhedral), quartz (rounded, considered partially resorbed), and albite (subhedral) appear to be the earliest minerals to crystallize in most samples from granite layers. The texture of the albite in these layers is consistent with a magmatic origin rather than metasomatic introduction of Na (albitization). Garnet may also have been an early liquidus phase. Microcline, on the other hand, most commonly occurs interstitially to the previously mentioned minerals. Muscovite commonly forms fairly large, ragged laths that cross-cut feldspar and show vermicular intergrowths with quartz. Its relative position in the paragenetic sequence is equivocal, but it is possible that at least some muscovite is of very late, even subsolidus, origin.

In the pegmatite layers, perthite and tourmaline commonly show evidence of nucleation at or near the contacts of the layer, with subsequent growth oriented approximately normal to the contact. Many crystals exhibit increasing size into the layer in the direction of growth. These "unidirectional solidification textures" (Shannon *et al.* 1982) are more common on hanging-wall contacts, suggesting crystallization from the top down, but they have been observed on footwall contacts as well, indicating that some pegmatite layers crystallized inward from both contacts.

Millimeter-scale layers (line rock)

The fine-grained portions of textural layers commonly show a distinctive internal layering consisting of alternating laminae, 2–20 mm thick, containing concentrations of light and dark minerals, a feature termed "line rock" by Schaller (1925). Rockhold *et al.* (1987) presented data on the mineralogy and chemistry of this type of layering at Calamity Peak, and Duke *et al.* (1988) reviewed structural and textural features of layering at this scale. The sequence of repeated laminations may reach 50 cm or more in thickness, usually comprising the whole of the host granite layer. The laminations are concordant to the lower (and usually the upper) contact of the enclosing granite layer, and they can be traced laterally along most of its length. In samples of line rock from Calamity Peak, dark layers are always defined by a relative concentration of tourmaline (up to ~7 vol.%), usually accompanied by increased quartz, microcline, and garnet relative to adjacent light-colored layers. Light layers show a complementary enrichment in albite (up to ~70 vol.%), and possibly also muscovite, compared to the dark layers. The laminae reflect changes in mineral abundance only, with little or no variation in the chemical composition of the individual phases (Rockhold *et al.* 1987).

Perthite megacrysts occur in some varieties of line rock, and these typically broaden upward from the footwall toward the hanging wall. Duke *et al.* (1988) cited this upward broadening of the megacrysts, along with examples of deflections in line-rock laminations over the top of some crystals, as evidence that growth of the megacrysts and crystallization of the line rock proceeded from the footwall toward the hanging wall. Redden (1963) and Jahns & Tuttle (1963) described similar features and reached the same conclusions with respect to upward crystallization.

Fracture-filling units

At least four compositionally, texturally, and structurally distinct types of fracture-filling bodies cross-cut the layered sequence at Calamity Peak (Duke *et al.* 1988). In order from apparently oldest to youngest, these are: (1) pegmatitic fracture-fillings, similar in texture and mineralogy to the pegmatite layers; (2) coarse graphic perthite fracture-fillings, composed almost entirely of graphic-textured perthite in crystals that average 0.3–1.0 m across; (3) rose quartz - perthite fracture-fillings; and (4) aplite fracture-fillings. Types 1 and 3 are generally 0.1–1.0 m thick, whereas type 2 may reach up to 5 m or more across, and type 4 is generally about 0.1 m across.

Feeder sills

Pegmatitic sills are common in the country rock that forms the floor of the exposed portions of the pluton (Duke *et al.* 1988, Fig. 2, cross section). These merge upward into the main mass of the pluton along the discordant lower contact, and may have served as conduits for part of the magma that fed the pluton.

PETROGRAPHY OF ROCK-TYPES ANALYZED IN THIS STUDY

Pegmatitic layers are enriched in megacrysts of perthite that, in extreme cases, measure up to 1 m in maximum dimension. Fine-grained quartz, albite, muscovite, tourmaline, and garnet make up the remainder of the rock; locally, these are accompanied by trace amounts of apatite, sillimanite, arsenopyrite, beryl, and graphite. Fine-grained layers contain a higher proportion of albite relative to perthite, are typically equigranular, and have grain sizes of about 2 mm or less. Geochemical analyses in this report pertain to three types of fine-grained layers as described below.

Line rock is distinguished by rhythmic laminations in color, and contains quartz, albite, tourmaline, and K-feldspar (microcline), with lesser amounts of muscovite, garnet, and, more rarely, apatite. Sillimanite, chrysoberyl, and monazite also have been identified.

Nonlaminated granites also occur as fine-grained layers. In general, the mineralogy is identical to that of line rock; however, the grain size is typically slightly coarser. Apatite is a common accessory phase, and chrysoberyl occurs in one sample.

Biotite granite makes up less than 5% of the exposed rock. Like line rock and nonlaminated granite, it occurs interlayered with pegmatitic granite; however, the biotite granite lacks internal laminations, and contains biotite to the virtual exclusion of tourmaline. In one 25-cm-thick intrusive layer, biotite granite grades upward continuously into tourmaline granite in the apparent direction of crystallization. Biotite granite is the only common rock-type noted for a conspicuous content of apatite, on the order of 0.1–0.2 vol.%. Other accessories minerals are zircon, sillimanite, and graphite.

Aplite dikes are composed of quartz, albite, K-feldspar, and muscovite. Both tourmaline-rich and tourmaline-free types occur; other accessories include garnet, apatite, zircon, monazite, and columbite.

Feeder sills are similar in mineralogy to the pegmatite layers except for the presence of minor biotite, and slightly greater proportions of apatite, sillimanite, and graphite.

ANALYTICAL METHODS

Samples weighing approximately 3–7 kg were homogenized for whole-rock chemical analyses; the large size of sample was used in an attempt to obtain representative measurements on coarse-grained rock-types. Samples were analyzed by a combination of energy-dispersion X-ray fluorescence, atomic absorption spectroscopy, and instrumental neutron activation analysis at Battelle Pacific Northwest Laboratories following methods described in Shearer *et al.* (1986) and Laul (1979). Loss on ignition was measured at 900°C for most samples. In addition, B and P were determined by direct-current plasma spectroscopy at X-ray Assay Laboratories, Don Mills, Ontario.

WHOLE-ROCK GEOCHEMISTRY

All samples from the Calamity Peak pluton are granitic in composition and contain 70–76 wt.% SiO_2. All samples are corundum-normative and have A/CNK $\geq$ 1.1 [where A/CNK = molar $Al_2O_3/(CaO+Na_2O+K_2O)$ after CaO is adjusted for the formation of normative apatite]. (Note that the value of A/CNK is lowered by 0.05, on average, if no correction is made for apatite; this practice may be appropriate for some of these samples, which seem to contain little or no apatite.) Major-element compositions, CIPW norms, and mineral assemblages of representative samples are given in Table 1A. Data on minor- and trace-element abundances are listed in Table 2A. Listed compositions include samples of the principal rock-types described above, as well as a range of lateral positions within the layered sequence of the granite–pegmatite complex. Average compositions of the principal rock-types are compared with that of average Harney Peak biotite granite in Figure 3, which shows relative enrichment or depletion patterns for 41 major, minor, and trace elements.

Coexisting granite and pegmatite layers were sampled at five locations in the Calamity Peak pluton in an attempt to isolate the effects of mineralogical segregation on element partitioning between granite and pegmatite layers from other types of fractionation. Samples selected to evaluate this aspect of the geochemistry were examined carefully in the field for evidence that they were representative of coexisting layers. All but one pair of samples were found to be in direct contact, and in all but one pair the pegmatite sample was found to be structurally above the granite, in accord with the genetic interpretations of Jahns & Tuttle (1963) and Duke *et al.* (1988). The major-element chemistry and mineralogy of coexisting granite and pegmatite layers at these five locations are included in Table 1B, and corresponding trace-element data

TABLE 1A. REPRESENTATIVE COMPOSITIONS FROM THE CALAMITY PEAK PLUTON AND AVERAGE HARNEY PEAK BIOTITE GRANITE

Sample	CP84	CP85	CP61	CP123	CP60	CP101	CP46	CP108	CP90	CP124	CP91	CP76	CP121	CP115	CP43	CP40	Avg.
Type[1]	LFS	UFS	LR1	LR1	LR2	LR2	LR3	PL3	PLCR	BG1	BG2	BG2	G2	G3	A2	A2	HPBG
SiO_2 wt.%	71.6	70.6	75.0	74.1	75.0	73.0	74.0	73.2	72.7	72.4	72.7	74.0	73.6	73.0	74.5	72.9	72.9
TiO_2	0.050	0.030	0.012	0.010	0.010	0.011	0.010	0.015	0.040	0.030	0.020	0.011	0.005	0.011	0.010	<0.01	0.093
B_2O_3	0.09	0.03	0.41	0.31	0.40	0.41	0.44	0.22	0.02	0.10	0.02	0.02	0.01	0.36	0.03	0.31	0.01
Al_2O_3	18.0	16.0	14.5	14.3	15.5	16.0	15.5	15.0	16.0	14.6	16.0	15.2	14.3	14.1	16.0	15.5	14.6
FeO	0.94	0.50	0.64	0.63	0.63	0.77	0.81	0.57	0.32	0.81	0.77	0.55	0.45	0.72	0.87	0.86	0.90
MnO	0.060	0.020	0.025	0.023	0.020	0.025	0.030	0.015	0.006	0.022	0.010	0.026	0.080	0.010	0.035	0.040	0.012
MgO	0.12	0.06	0.10	0.12	0.08	0.13	0.08	0.10	0.10	0.14	0.13	0.07	0.03	0.13	0.06	0.09	0.17
CaO	0.20	0.33	0.30	0.65	0.54	0.80	0.40	0.30	1.00	0.62	1.00	0.77	0.30	0.33	0.45	0.47	0.98
Na_2O	2.45	3.34	4.20	6.30	6.60	6.75	6.00	4.00	5.10	5.40	6.25	6.80	5.20	3.61	3.00	5.00	3.78
K_2O	6.20	6.00	4.80	1.30	0.76	0.91	2.40	5.30	2.63	2.30	1.73	0.90	4.30	5.80	3.75	3.50	4.68
P_2O_5	0.22	0.19	0.24	0.21	0.25	0.22	0.27	0.22	0.20	0.25	0.17	0.20	0.26	0.18	0.48	0.39	0.15
Loss on ignition	1.0	0.8		0.7		0.5		0.5	0.9	1.0	0.8		0.3	0.4			
TOTAL	99.9	97.1	100.2	98.0	99.8	99.0	99.9	98.9	98.1	96.7	98.8	98.5	98.5	98.3	99.2	99.1	98.3
CIPW norm (wt.%)																	
Q	32.83	27.53	31.54	30.96	32.59	28.31	29.00	29.00	31.00	30.68	27.23	29.34	26.50	28.81	42.26	29.63	30.38
or	36.64	35.46	28.37	7.68	4.49	5.38	14.18	31.32	15.54	13.59	10.22	5.32	25.41	34.28	22.16	20.68	27.66
ab	20.73	28.26	35.54	53.31	55.85	57.12	50.77	33.85	43.16	45.69	52.89	57.54	44.00	30.55	25.39	42.31	31.99
an	0	0.40	0	1.85	1.05	2.53	0.22	0.05	3.65	1.44	3.85	2.51	0.00	0.46	0.00	0.00	3.88
C	7.42	3.87	2.42	1.85	3.44	2.98	2.95	2.66	3.42	2.70	2.44	2.12	1.17	1.71	7.34	3.57	1.89
hy	2.05	1.06	1.45	1.48	1.38	1.77	1.73	1.30	0.78	1.83	1.72	1.21	1.05	1.65	1.78	1.86	1.94
il	0.09	0.06	0.02	0.02	0.02	0.02	0.02	0.03	0.08	0.06	0.04	0.02	0.00	0.02	0.02	0.02	0.18
ap	0.51	0.44	0.56	0.49	0.58	0.51	0.63	0.51	0.46	0.58	0.39	0.46	0.60	0.42	1.11	0.90	0.35
Total	100.27	97.08	99.90	97.64	99.40	98.62	99.50	98.72	98.09	96.57	98.78	98.52	98.73	97.90	100.06	98.97	98.27
$Na_2O/(Na_2O+K_2O)$	0.28	0.36	0.47	0.83	0.90	0.88	0.71	0.43	0.66	0.70	0.78	0.88	0.55	0.38	0.44	0.59	0.45
A/CNK	1.7	1.3	1.2	1.1	1.3	1.2	1.2	1.2	1.3	1.2	1.2	1.2	1.1	1.1	1.8	1.3	1.1
Mineral assemblage[2]	Kfs,Qtz, Ab,Ms, Sil,Bt, Tur,Grt, Gr	Qtz,Kfs, Ab,Ms, Sil,Tur, Grt,Ap, Gr	Kfs,Qtz, Ab,Tur, Grt,Ms	Ab,Qtz, Kfs,Tur, Grt,Ms	Ab,Qtz, Tur,Ms, Kfs,Grt	Ab,Qtz, Kfs,Tur, Ms,Grt, Ap,Sil	Ab,Qtz, Kfs,Tur, Ms,Grt, Ap	Ab,Qtz, Kfs,Ms, Tur,Grt, Ap,Sil	Ab,Qtz, Ms,Tur, Ap	Ab,Qtz, Kfs,Ms, Bt,Tur, Grt,Ap	Ab,Qtz, Mc,Ms, Bt,Ap, Tur,Grt, Sil,Gr	Ab,Qtz, Kfs,Ms, Bt,Grt, Ap	Kfs,Qtz, Ab,Grt, Ms,Cbr	Qtz,Kfs, Ab,Tur, Ms,Grt, Ap	Ab,Qtz, Ms,Ap, Zrn,Clm	Ab,Qtz, Kfs,Ms, Tur,Grt, Ap,Mnz, Zrn	

1 Rock type codes: LFS, UFS, lower and upper feeder sills; LR, line rock; PL, pegmatite layer; BG, biotite granite; G, non-laminated granite lacking significant biotite; A, aplite; PLCR, pegmatite layer (sill) in country rock. Numbers 1-3 indicate location of sample in low (1), middle (2), or upper (3) megalayer (see Duke et al. 1988). Avg. HPBG, average of 4 Harney Peak biotite granites.

2 Listed in order of decreasing abundance. Mineral abbreviations -- Qtz, quartz; Kfs, K-feldspar; Ab, albite; Ms, muscovite; Tur, tourmaline; Bt, biotite; Grt, garnet; Ap, apatite; Sil, sillimanite; Gr, graphite; Zrn, zircon; Mnz, monazite (Kretz 1983). Cbr, chrysoberyl; Clm, columbite.

TABLE 1B. MAJOR-ELEMENT CHEMISTRY OF COEXISTING GRANITE AND PEGMATITE LAYERS FROM THE CALAMITY PEAK PLUTON

Sample Type[1]	CP105 LR3	CP106B PL3	CP113 LR3	CP114 PL3	CP122 LR2	CP120 PL2	CP63 LR2	CP64 PL2	CP126 LR3	CP127 PL3
SiO_2 wt.%	73.5	74.7	73.0	70.8	74.6	74.2	75.3	74.7	72.7	75.8
TiO_2	0.012	0.010	0.010	0.005	0.015	0.020	0.010	0.010	0.011	0.012
B_2O_3	0.56	0.15	0.49	0.08	0.59	0.21	0.25	0.18	0.52	0.51
Al_2O_3	14.4	14.8	14.9	15.5	14.7	14.5	14.8	14.5	14.6	13.5
FeO	0.90	0.45	0.63	0.33	0.81	0.63	0.50	0.36	0.81	0.83
MnO	0.031	0.022	0.018	0.009	0.013	0.034	0.014	0.010	0.020	0.021
MgO	0.17	0.07	0.08	0.04	0.13	0.10	0.08	0.06	0.12	0.10
CaO	0.60	0.34	0.35	0.21	0.45	0.30	0.60	0.30	0.52	0.40
Na_2O	5.45	4.15	6.20	4.10	6.90	4.41	6.50	4.60	6.45	5.40
K_2O	2.52	5.50	2.90	7.00	0.90	3.60	1.00	4.05	1.15	2.30
P_2O_5	0.18	0.22	0.36	0.40	0.28	0.32	0.17	0.13	0.24	0.25
Loss on ignition	0.40	0.40	0.40	0.51	0.50	0.70			0.50	0.40
Total	98.3	100.4	98.9	98.5	99.4	98.3	99.2	98.9	97.1	99.1
CIPW norm (wt.%)										
Q	30.35	28.91	25.45	20.49	29.97	34.34	32.32	31.77	29.48	34.58
or	14.89	32.50	17.14	41.37	5.32	21.28	5.91	23.93	6.80	13.59
ab	46.12	35.12	52.46	34.69	58.39	37.32	55.00	38.92	54.58	45.69
an	1.80	0.25	0.00	0.00	0.40	0.00	1.87	0.64	1.01	0.35
C	2.05	1.93	1.79	1.75	2.23	3.57	2.34	2.32	2.37	2.00
hy	2.11	1.03	1.37	0.72	1.81	1.44	1.13	0.81	1.81	1.79
il	0.02	0.02	0.02	0.00	0.03	0.04	0.02	0.02	0.02	0.02
ap	0.42	0.51	0.83	0.93	0.65	0.74	0.39	0.30	0.56	0.58
Total	97.76	100.27	99.06	99.95	98.80	98.73	98.98	98.71	96.63	98.60
$Na_2O/(Na_2O+K_2O)$	0.68	0.43	0.68	0.37	0.88	0.55	0.87	0.53	0.85	0.70
A/CNK	1.2	1.2	1.1	1.1	1.2	1.3	1.2	1.2	1.2	1.2
Mineral assemblage[2]	Qtz,Kfs, Ab,Tur, Ms,Grt	Qtz,Ab, Kfs,Ms, Tur,Grt, Sil,Ap	Ab,Qtz, Kfs,Tur, Ms,Grt, Cbr	Ab,Qtz, Kfs,Ms, Tur,Grt, Sil,Brl	Ab,Qtz, Tur,Kfs, Ms,Grt	Qtz,Kfs, Ab,Ms, Tur,Grt, Sil,Ap, Gr	Ab,Qtz, Tur,Kfs, Ms,Grt, Ap	Qtz,Kfs, Ab,Ms, Tur,Grt	Ab,Qtz, Kfs,Tur, Ms,Grt,	Qtz,Ab, Kfs,Tur, Ms,Grt, Ap

[1] Rock type codes same as in Table 1A. Successive LR-PL samples coexist in single outcrop.

[2] Listed in order of decreasing abundance. Mineral abbreviations as in Table 1A, with the addition of Brl, beryl (Kretz 1983), and Cbr, chrysoberyl.

are given in Table 2B. These results are summarized graphically in Figure 4, which shows enrichment factors (designated as concentration in pegmatite divided by concentration in granite) for 41 elements for each coexisting pair.

Major elements

The data in Tables 1A and 1B illustrate that samples from the Calamity Peak pluton all contain 88% or more normative quartz (Q), albite (Ab), and orthoclase (Or) components. Thus the overall major-element chemical variations among samples are conveniently approximated by reference to the haplogranite system (Fig. 5). Six of the samples depicted in Figure 5A were too coarse grained to obtain a representative sample for geochemistry. In these cases, the plotted composition is calculated from point counts in the field (200–1000 counts using a 10-cm grid) combined with chemical data on minerals from the same outcrop or similar outcrops and published mineral densities for the appropriate compositions.

Figure 5 indicates that, although some compositions at Calamity Peak cluster around the thermal minima in the water-saturated haplogranite system (± added B_2O_3), there is a wide range in composition, especially in the Ab–Or ratio. For the most part, the analyzed material does not have a "minimum melt" composition. This discrepancy would be exaggerated if the H_2O-undersaturated minima were considered, since these plot closer to Or, whereas the Calamity Peak data are skewed toward more sodic compositions.

Much of the major-element variation correlates with rock-type; for example, Figure 5b shows the compositions of coexisting granite and pegmatite layers in terms of normative Q–Ab–Or. As anticipated, the relatively K-rich pegmatite layers invariably have higher Or content than associated granite layers (*e.g.*, Jahns & Tuttle 1963, Fig. 10). It can also be seen, however, that granite layers with the lowest Or content tend to coexist with pegmatite of low Or content. Pegmatite layers have slightly higher Q/Ab than coexisting granite layers, and as the average Or content of the pairs decreases, this difference becomes more

TABLE 2A. MINOR- AND TRACE-ELEMENT ANALYSES OF SAMPLES FROM THE CALAMITY PEAK PLUTON AND AVERAGE HARNEY PEAK BIOTITE GRANITE[1]

Sample	CP84	CP85	CP61	CP123	CP60	CP101	CP46	CP108	CP90	CP124	CP91	CP76	CP121	CP115	CP43	CP40	Avg.
Type[2]	LFS	UFS	LR1	LR1	LR2	LR2	LR3	PL3	PLCR	BG1	BG2	BG2	G2	G3	A2	A2	HPBG
Sc			0.45	0.80	0.35	0.53	0.40	1.00		1.50	0.80		0.50	0.60			3.00
Cr	20	20	20	30	25	20	20	30	<20	30	26	30	25	30	25	30	21
Co			0.18	0.28	0.12	0.32	0.12	0.21		0.32	0.29		0.23	0.29			0.70
Ni	3	2.7	<4	4.1	<4	<3	<4	3.7	<2	2.6	2.3	<4	3.6	<3	<4	<4	5.1
Cu	8.0	7.8	5.1	8.9	6.0	5.5	4.4	5.5	9.9	5.4	5.5	5.4	6.7	6.6	6.0	6.4	9.5
Zn	20.3	7.3	32.0	27.4	31.0	26.0	52.0	21.5	7.7	21.0	30.0	20.0	5.7	32.0	38.0	51.0	27.5
Ga	19.4	19.3	12.7	14.2	16.3	14.4	17.4	16.1	15.4	19.0	19.0	15.4	14.4	16.2	52.0	25.0	19.2
As	9.7	3.8	61.5	18.9	7.6	2.5	10.1	<1.6	10.4	23.6	6.9	11.7	2.5	<1.6	4.5	25.4	1.6
Rb	250	225	215	48	11.4	20.1	160	260	120	106	100	39.0	230	200	1090	480	160
Sr	36	44	17	34.0	12	31	11	25.0	150	35.4	32	24	22.0	27.0	200	21	86
Y	5.4	4.5	3.2	2.2	2.4	8.0	4.5	4.1	4.5	10.9	5.0	6.1	3.4	3.7	5.4	6.4	10.0
Zr	38	12.9	33.0	26.1	29.0	33.4	30.0	9.2	120	25.0	21.0	24	21.0	26.7	28.4	11.3	89
Nb	12.3	9.0	<2	3.2	<2	1.2	<2	4.9	12.9	10.2	12.1	5.9	4.8	2.2	150	21.3	7.7
Mo	<1	<1	<2	<1	<2	<1	<2	<1	<1	1.5	<1	<2	<1	<1	<2	<2	3.2
Sn	16	13		8.3		<7		10	17	<7	<7		<7	<7			
Sb			0.190	0.090	0.030	0.050	0.180	0.080		0.060	0.030		0.240	0.060			0.05
Cs			5.0	2.3	0.45	3.9	2.2	9.60		5.00	4.50		4.50	15.50	180	80	3.0
Ba	370	210	30	20	<10	<20	<10	50	310	30	20	<10	30	40	22	20	360
La			0.90	0.90	1.55	1.90	1.30	0.75		2.30	2.90		0.90	1.10			22.3
Ce			1.9	1.9	2.9	4.4	3.0	1.6		5.4	6.1		2.0	2.4			44.6
Nd			1.0	0.85	1.2	2.4	1.3	0.7		3.1	2.8		1.1	1.3			21.5
Sm			0.15	0.080	0.14	0.60	0.19	0.12		0.68	0.53		0.15	0.22			4.5
Eu			0.041	0.095	0.030	0.083	0.015	0.090		0.15	0.13		0.035	0.12			0.48
Gd			0.22	0.15	0.47	0.60	0.58	0.20		0.91	0.85		0.26	0.27			6.1
Tb			0.050	0.030	0.053	0.220	0.075	0.058		0.24	0.16		0.060	0.075			0.51
(Ho)			(0.30)	(0.20)	(0.30)	(0.55)	(0.53)			(0.31)	(0.60)		0.26	(0.30)			(0.52)
(Tm)			0.032	0.053	0.040	0.10	0.040	0.050		0.14	0.12		0.070	0.045			0.090
Yb			0.25	0.31	0.25	0.69	0.27	0.19		0.71	0.31		0.20	0.30			0.49
Lu			0.050	0.052	0.045	0.10	0.067	0.041		0.10	0.046		0.045	0.050			0.050
Hf			1.6	1.3	1.3	1.4	1.7	0.50		1.1	1.0		1.2	1.3			2.7
Ta			0.20	0.82	0.45	0.18	0.54	0.82		1.20	2.50		1.15	0.23			0.53
Pb	38.6	38.6	39.0	31.0	32.0	24.2	29.0	44.5	51.2	29.0	35.0	31.6	34.3	44.0	15.0	27.0	44.0
Th			0.43	0.36	0.68	1.10	0.55	0.26		0.73	1.5		0.73	0.90			20.7
U			2.5	1.1	2.2	3.0	4.9	1.1	7.5	2.4	2.9	6.5	1.8	1.9	30	15	5.3
K/Rb	206	221	185	225	553	376	124	169	182	180	144	192	155	241	29	61	243
Rb/Sr	6.9	5.1	12.6	1.4	1.0	0.65	14.5	10.4	0.8	3.0	3.1	1.6	10.5	7.4	5.5	22.9	1.9
Rb/Cs			43	21	25	5.2	73	27		21	22		51	13	6.0	6.0	53
Ba/Cs			6.0	8.7				5.2		6.0	4.4		6.7	2.6	0.10	0.30	120
Ba/Sr	10.3	4.8	1.76	0.59				2.0	2.07	0.85	0.63		1.36	1.48	0.11	0.95	4.19
Zr/Hf			21	20	22	24	18	18		23	21		18	21			33
Zr/Y	7.0	2.9	10.3	11.9	12.1	4.2	6.7	2.2	26.7	2.3	4.2	3.9	6.2	7.2	5.3	1.8	8.9
La_n/Lu_n		1.9	1.8	2.1	2.0	2.0	2.2	1.9		2.4	6.5		2.1	2.3			46.0
Eu/Eu*[3]			0.69	2.7	0.36	0.43	0.14	1.8		0.59	0.60		0.54	1.51			0.28
Th/U			0.17	0.33	0.31	0.37	0.11	0.24		0.30	0.52		0.41	0.47			3.91

1 Concentrations in ppm. Also analyzed but not reported: V < 20 ppm. 2 Rock type codes same as in Table 1A. 3 Eu* obtained by interpolating between Sm and Gd on chondrite-normalized pattern.

pronounced, so that tie-lines rotate in a counterclockwise fashion.

Other coarse-grained rock-types follow a trend of Or enrichment similar to that shown by pegmatite layers; these include analyzed compositions of the upper portions of the feeder sills, and compositions calculated by the modal recombination method for pegmatite layers, pegmatitic fracture-filling units, and coarse graphic perthite fracture-filling units.

Despite the wide range in the Ab–Or ratio in samples from Calamity Peak, the average values for the principal rock-types are generally significantly more sodic than average Harney Peak biotite granite, with a complementary relative depletion in K (Fig. 3). Among the other major elements, the Calamity Peak samples are depleted in Ca, Fe, Mg, and Ti, but enriched in Mn, irrespective of rock-type. For most rock-types, fractionation of Si and Al is insignificant in comparison to analytical uncertainties ($\leq$ 2% relative increase in SiO_2; $\leq$ 3% relative increase in Al_2O_3).

The variation in major-element composition of the Calamity Peak rocks also is shown in AFM and AFK diagrams (Fig. 6). In the AFM diagrams (Figs. 6A, B), there is considerable overlap among different rock-types. All of the highly aluminous samples plotting at greater than 80% "A", are coarse-grained rocks (pegmatite layers or feeder sills) or aplites. The anomalous point with low "A" and high "M" is a sample of tourmaline-rich line rock with the highest MgO of any sample and relatively low Al_2O_3. The tourmaline exhibits highly variable Fe/Mg (Rockhold *et al.* 1987), but generally has the highest "M" value of the ferromagnesian phases.

TABLE 2B. MINOR- AND TRACE-ELEMENT DATA ON COEXISTING GRANITE AND PEGMATITE LAYERS FROM THE CALAMITY PEAK PLUTON[1]

Sample	CP105	CP106B	CP113	CP114	CP122	CP120	CP63	CP64	CP126	CP127
Type[2]	LR3	PL3	LR3	PL3	LR2	PL2	LR2	PL2	LR3	PL3
Sc	0.53	0.45	0.50	0.35	0.37	1.10	0.38	0.91	0.45	0.45
Cr	30	15	25	25	22	40	25	20	30	25
Co	0.48	0.38	0.19	0.21	0.20	0.22	0.16	0.13	0.20	0.20
Ni	<3	3	3.2	3.2	<3	<3	<4	<4	<3	<2
Cu	6.1	6.4	5.0	7.0	5.4	5.4	6.5	5.0	4.6	6.0
Zn	33.4	10.5	45.0	15.7	51.7	23.7	20.0	14.0	50.3	57.0
Ga	14.9	12.7	17.0	16.8	16.0	22.4	12.6	12.0	15.0	16.1
As	<1.4	1.7	<1.4	4.4	<1.3	3.1	5.5	25.0	3.1	11.6
Rb	90.0	220	175	550	19.0	240	30	160	26.4	87.0
Sr	25.0	27.0	22.8	50.4	47.0	48.3	24	20	22.4	19.0
Y	6.7	4.3	3.2	3.3	3.9	3.4	2.8	4.0	6.4	3.6
Zr	46.5	17.1	18.4	5.8	26.2	22.3	25.0	28.7	21.5	14.0
Nb	1.5	1.8	3.5	6.8	<1	19.3	<2	2.6	<1	1.4
Mo	<1	<1	<1	1.7	<1	2	<2	<2	<1	<1
Sn	<7	<7	10	10	<7	15			<7	<7
Sb	0.050	0.070	0.030	0.060	<.04	0.060	0.060	0.050	0.050	0.050
Cs	2.1	5.8	1.9	18.8	0.64	9.0	1.1	3.5	0.75	3.4
Ba	40	60	<20	25	<20	20	35	90	<20	<20
La	2.70	1.40	0.75	0.35	1.00	0.75	1.20	1.40	1.70	1.55
Ce	5.5	2.5	1.6	0.80	2.4	1.6	2.5	3.2	4.0	3.5
Nd	2.8	1.2	0.85	<0.5	1.1	0.93	1.4	1.6	1.7	1.4
Sm	0.55	0.20	0.13	0.035	0.18	0.11	0.15	0.18	0.30	0.23
Eu	0.11	0.10	0.035	0.025	0.040	0.030	0.096	0.080	0.045	0.035
Gd	0.67	0.26	0.45		0.47	0.24	0.20	0.30	0.61	0.56
Tb	0.17	0.080	0.070	0.020	0.098	0.048	0.044	0.058	0.17	0.10
(Ho)						0.20				
(Tm)	0.089	0.072	0.040	0.030	0.033	0.070	0.039	0.071	0.055	0.030
Yb	0.70	0.40	0.24	0.070	0.23	0.17	0.35	0.46	0.32	0.18
Lu	0.11	0.066	0.043	0.015	0.050	0.035	0.080	0.089	0.052	0.030
Hf	2.4	0.77	0.87	0.20	1.2	1.1	1.0	1.0	1.0	0.70
Ta	0.15	0.45	1.00	1.50	0.05	1.90	0.20	0.65	0.16	0.23
Pb	33.5	48.5	30.3	37.6	24.3	26.5	36.0	50.0	22.2	23.0
Th	1.40	0.45	0.28	0.10	0.48	0.30	0.36	1.30	0.57	0.52
U	3.2	1.5	1.8	0.90	1.8	1.4	3.3	4.3	2.0	1.8
K/Rb	232	207	138	106	393	124	277	210	361	219
Rb/Sr	3.6	8.1	7.7	10.9	0.40	5.0	1.3	8.0	1.2	4.6
Rb/Cs	43	38	92	29	30	27	27	46	35	26
Ba/Cs	19	10.3		1.3		2.2	32	26		
Ba/Sr	1.62.2		0.50		0.41	1.5	4.5			
Zr/Hf	19	22	21	29	22	20	25	29	22	20
Zr/Y	6.9	4.0	5.8	1.8	6.7	6.6	8.9	7.2	3.4	3.9
La_n/Lu_n	2.5	2.2	1.8	2.4	2.1	2.2	1.5	1.6	3.4	5.3
Eu/Eu*[3]	0.56	1.3	0.45	1.7	0.42	0.57	1.7	1.1	0.32	0.30
Th/U	0.44	0.30	0.16	0.11	0.27	0.21	0.11	0.30	0.29	0.29

1 Concentrations in ppm. Also analyzed but not reported: V < 20 ppm.
2 Rock type codes same as in Table 1A.
3 Eu* obtained by interpolating between Sm and Gd on chondrite-normalized pattern.

The different rock-types are more readily differentiated on the AFK diagrams (Figs. 6C, D), with "line rock" and biotite granites plotting at higher "F" and generally higher "A", whereas pegmatite layers, aplite dikes, and "feeder sills" plot at lower "F" and generally higher "K".

Minor and trace elements

Concentrations of minor and trace elements of representative samples are given in Tables 2A and 2B. Figure 3 indicates the relative magnitude of enrichment or depletion of individual trace elements compared with average Harney Peak biotite granite for each of the principal rock-types. The most conspicuous difference is the enrichment of B by a factor of 5–80 in the rocks from Calamity Peak; even the biotite granites at Calamity Peak are enriched in B by a factor of about five. Boron enrichment corresponds with an overall abundance of tourmaline in most rock-types, although other minerals, especially muscovite, also may accommodate significant B (Rockhold *et al.* 1987). Phosphorus, As, and Sb also are enriched at Calamity Peak. Arsenopyrite has been observed as a trace constituent of some samples. Apatite occurs also, but is less conspicuous than in many parts of the Harney Peak Granite; it is possible that apatite stability is suppressed by the low Ca content at Calamity Peak, and that much of the P is accommodated by other minerals, such as feldspars (*e.g.*, London 1990).

Barium and Sr are depleted in all rock-types; Rb is depleted in biotite granite, biotite-poor granite, and line rock, but enriched in pegmatite layers, feeder sills, and, especially, in aplite. Cesium is depleted in line rock, but enriched in all other types for which data are available.

All light-rare-earth elements (*LREE*) and Th show an almost identical degree of depletion at Calamity Peak. Europium is less strongly depleted. Scandium, Y, U, and Pb are depleted, though much less strongly than Th, and the heavy rare-earths (*HREE*) progress fairly systematically from strongly depleted (Gd) to slightly enriched (Lu).

Rare-earth elements

Enrichment and depletion of individual *REE* relative to the average Harney Peak biotite granite were discussed briefly above (Fig. 3). Figure 7 is a chondrite-normalized *REE* diagram showing composite patterns for different rock-types at Calamity Peak compared with a composite of three samples of Harney Peak biotite granite.

In general, the Calamity Peak *REE* patterns have fairly flat slopes, with low overall abundances of the *REE*. Relative to the Harney Peak biotite granites, the Calamity Peak samples are one to two orders of magnitude depleted in the *LREE* (average normalized La_n/Lu_n = 48 and 2.6, respectively), with generally larger Eu/Eu* (average 0.28 and 0.71, respectively). With respect to individual rock-types from Calamity Peak (Fig. 8), biotite granites contain the highest concentration of all *REE* except for Yb and Lu. The pegmatite layers are distinguished by the lowest overall concentrations of the *REE*, and four of six samples of pegmatite layers have positive Eu anomalies.

Four of the samples of nonlaminated granite have patterns similar to those of the biotite granites; two of these contain a small amount of biotite. In a sequence of samples from a single outcrop, the *REE* concentrations decrease slightly in proportion to the ratio of tourmaline to biotite. In these samples, the order is 109 (5% Bt, 1.5% Tur; volume estimates) → 109B (1% Bt, 2% Tur) → 109A (no Bt, 4% Tur) → 110 (no Bt, 5% Tur). The remaining patterns in this category have distinctly lower *REE* concentrations and greater similarity with patterns for the pegmatite layers.

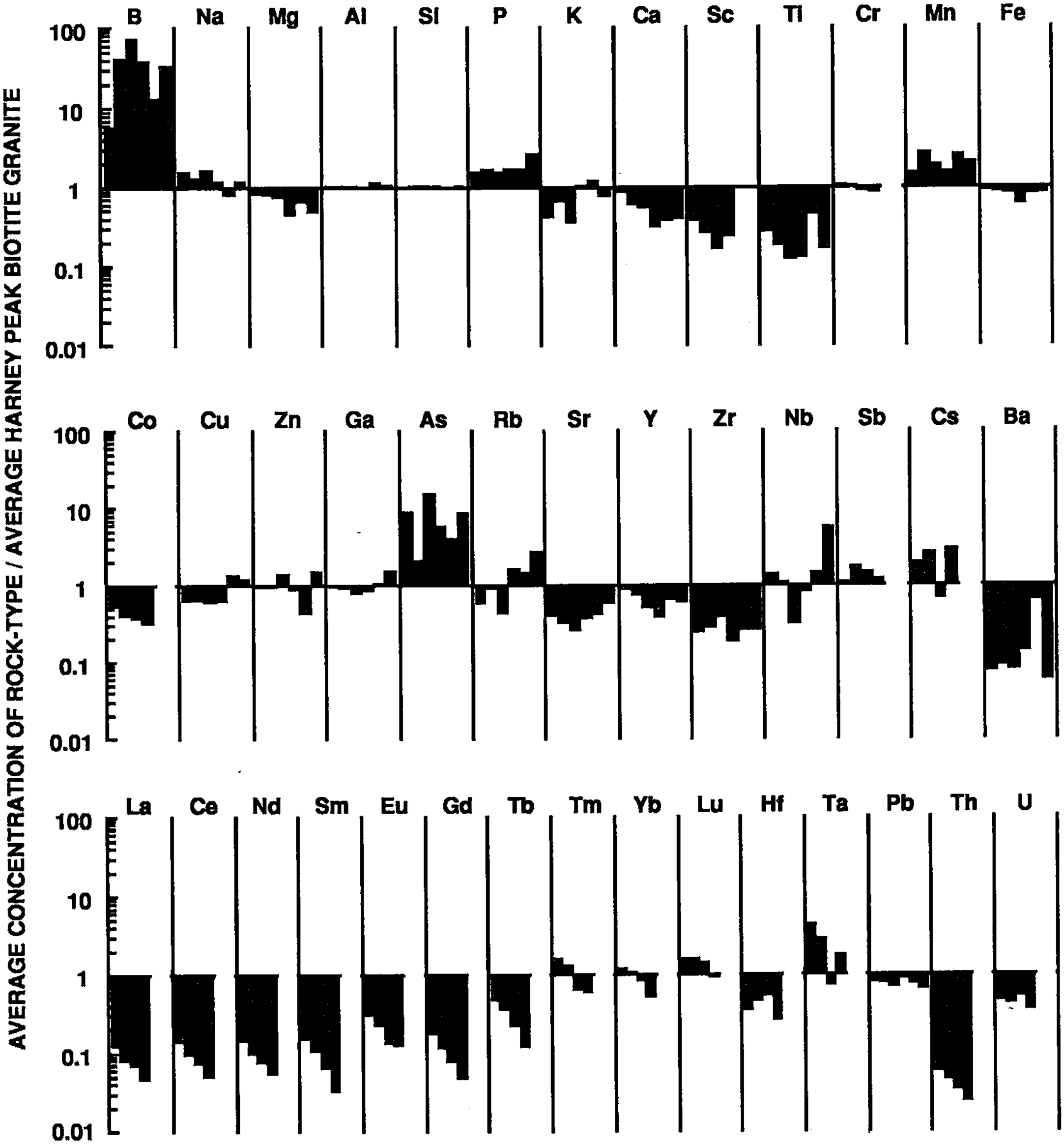

FIG. 3. Enrichment and depletion of averages for the six principal rock-types at Calamity Peak relative to an average of four Harney Peak biotite granites (unpublished results of C.K. Shearer and E.F. Duke). Order of rock-type columns is, from left to right: biotite granites ($n = 7$), nonlaminated biotite-poor granites ($n = 4$), line rock ($n = 20$), pegmatite layers ($n = 6$), feeder sills ($n = 4$), and aplites ($n = 6$). Blanks in graph denote missing or incomplete data.

The most complete *REE* data pertain to the laminated tourmaline granites (line rock). These have *REE* contents lower than the biotite granites but higher, in general, than associated pegmatite layers (Fig. 4). Two of twelve patterns have positive Eu anomalies.

Chemical variation between coexisting granite and pegmatite layers

Figure 4 shows consistent partitioning of almost all elements between granite and pegmatite layers. In addition to Na, mentioned above, all granite layers are relatively enriched in B, Ca, Fe, Mg, and Hf. In almost every case, granite layers are also

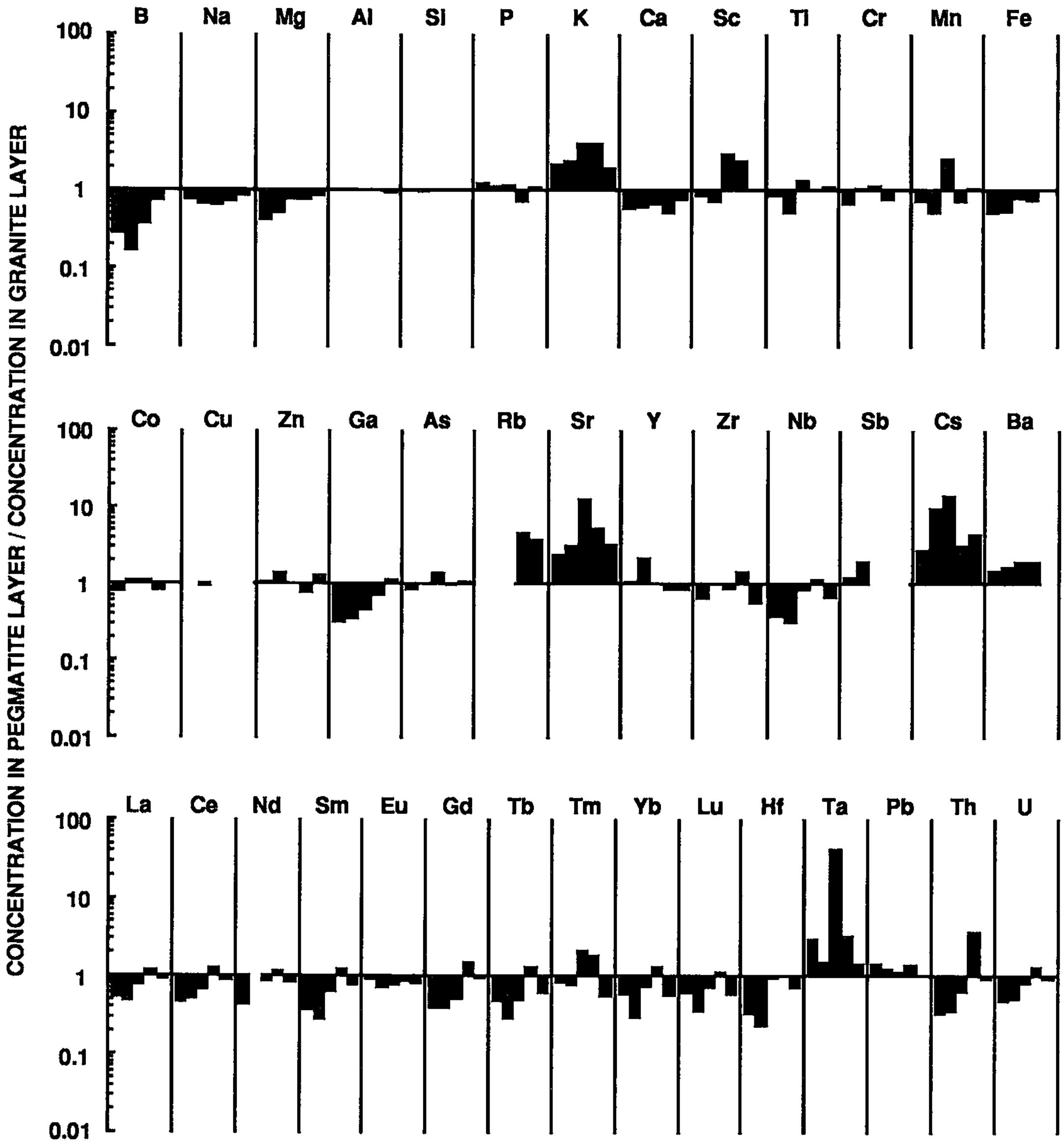

FIG. 4. Relative enrichment and depletion of selected elements in five pairs of coexisting granite and pegmatite layers in the Calamity Peak pluton. Enrichment factor for each element is defined by concentration in pegmatite divided by concentration in granite, so that values greater than one indicate elements enriched in pegmatite layers. Blanks in bar graphs denote missing or incomplete data. For each element, the order of sample pairs is, from left to right, the same as their order of listing in Tables 1B and 2B.

enriched in Mn, Zn, Y, Zr, Th, U, and all *REE*, with the possible exception of Tm. Pegmatite layers preferentially concentrate P, K, Rb, Cs, Ba, As, Ta, Nb, and Pb, and possibly Cu. Silicon and Al are not systematically fractionated between granite and pegmatite layers (compare Table 1B); however, the observed variations in these elements generally do not exceed the analytical precision. Variations of the remaining elements are poorly defined. One granite–pegmatite pair, CP63–CP64, is anomalous with respect to the bulk of the samples, showing reversals in partitioning of P, Y, Zr, Th, U, and all *REE* except Eu.

The ratios K/Rb, Sr/Rb, and Rb/Cs are consistently lower in coarse-grained layers than in coexisting fine-grained layers (Table 2B). Data on

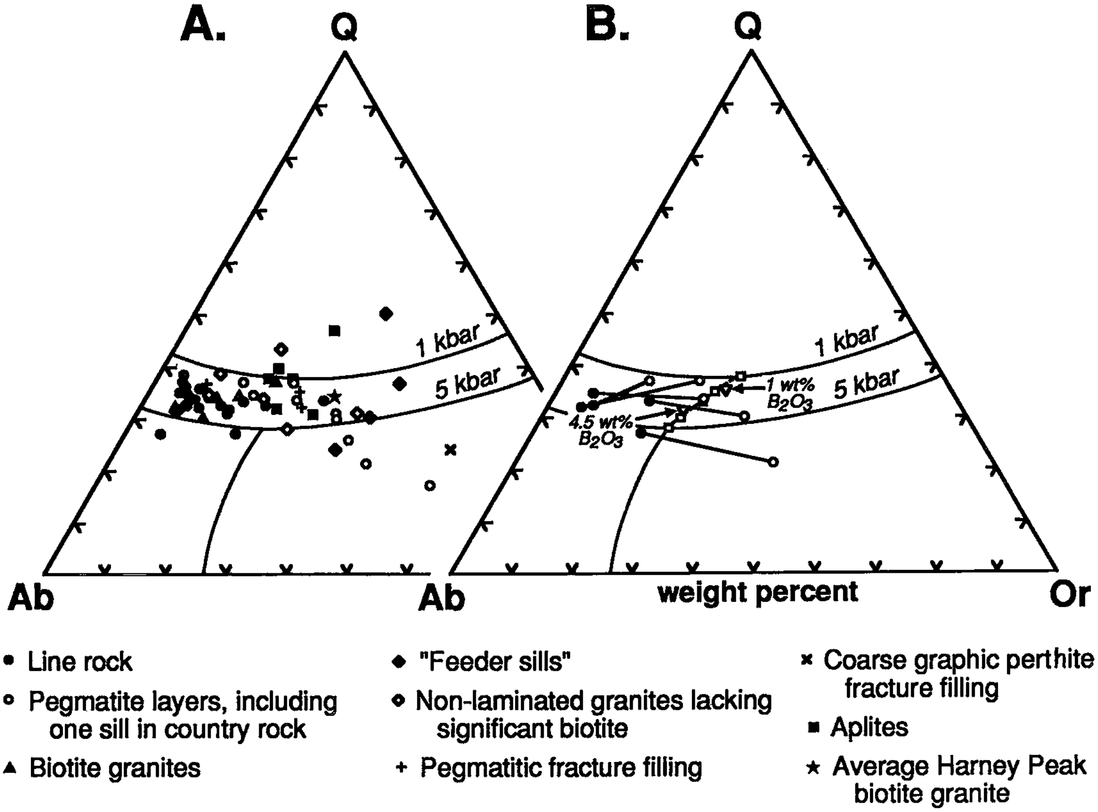

FIG. 5. Normative proportions of quartz (Q), albite (Ab), and orthoclase (Or) in samples from the Calamity Peak pluton. A. Calamity Peak samples shown by rock-unit type. Compositions of pegmatite fracture-fillings, coarse graphic perthite fracture-filling, and two of the pegmatite layers calculated by modal recombination (see text). B. Data for five pairs of coexisting granite–pegmatite layers. Tie lines connect coexisting samples from Table 1B. Open circles, pegmatite layer; filled circles, granite layer. Cotectics shown for $P(H_2O) = 1$ and 5 kbar, minima for $P(H_2O) = 1, 2, 3,$ and 4 kbar, and the 5-kbar eutectic (open squares in B) are from Luth *et al.* (1964). Pseudoternary minima for $P(H_2O) = 1$ kbar with 1 and 4.5 weight % added B_2O_3 (inverted, open triangles in B) from Pichavant (1981).

variation of other trace-element ratios are either incomplete or inconclusive.

The partitioning of rare-earth elements between coexisting granite and pegmatite layers is illustrated in Figure 4, and chondrite-normalized patterns are shown in Figure 8. All the granite–pegmatite pairs are characterized by low ΣREE abundances (La_n $<$ 10X chondrite) and fairly flat *REE* patterns (La_n/Lu_n in the range 1.5–5.3). In all but one pair of coexisting layers, the pegmatite layer has lower overall *REE* abundances, and equal or greater Eu/Eu^*. The one exception to the generalization that the granite layers have higher *REE* and smaller Eu anomalies is the pair 63–64 cited previously as displaying anomalous relative partitioning of P, Y, Zr, Th, and U.

DISCUSSION

Chemical relationship to other portions of the Harney Peak Granite

The Harney Peak Granite dome shows a general pattern of zonation with respect to mineralogy, mineral chemistry, whole-rock chemistry, and rock texture (Shearer *et al.* 1987, Duke *et al.* 1990). More equigranular, homogeneous varieties of granite, which have less fractionated chemical characteristics of minerals and whole rocks, occupy the central and southeastern portions of the dome. These are dominantly biotite granites with a K/Rb of 200 or greater. Toward the western, northern, and northeastern perimeters of the dome, including

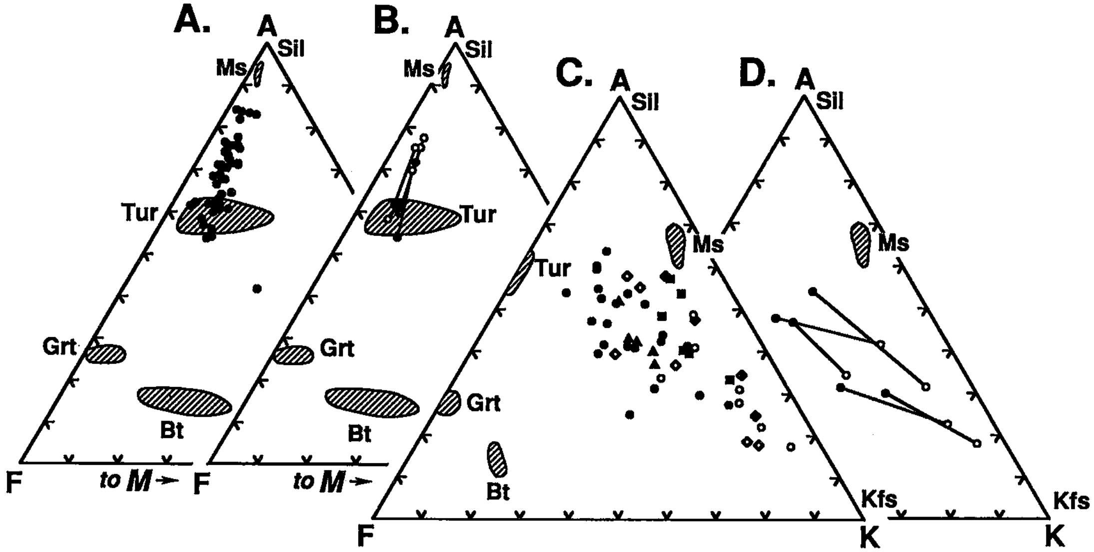

FIG. 6. AFM and AFK diagrams for rocks from the Calamity Peak pluton (A = Al_2O_3-K_2O-Na_2O-CaO, F = FeO+MnO, M = MgO, K = K_2O, molar basis; CaO is that remaining after subtraction of the appropriate amount for normative apatite). Diagonally ruled fields of minerals based on analyses of rocks from the Calamity Peak pluton (Rockhold *et al.* 1987 and unpublished analytical data of E.F. Duke) and the Harney Peak dome (unpublished data of C.K. Shearer). A. AFM diagram showing all samples from the Calamity Peak pluton. For clarity, all points shown with same symbol. B. AFM diagram showing only the distribution of coexisting granite and pegmatite layers. Open circles, pegmatite layers; filled circles, granite layers. C. AFK diagram showing samples by rock type. Symbols as in Fig. 5. D. AFK diagram showing the distribution of coexisting granite and pegmatite layers. Open circles, pegmatite layers; filled circles, granite layers. Mineral abbreviations given in footnote of Table 1A.

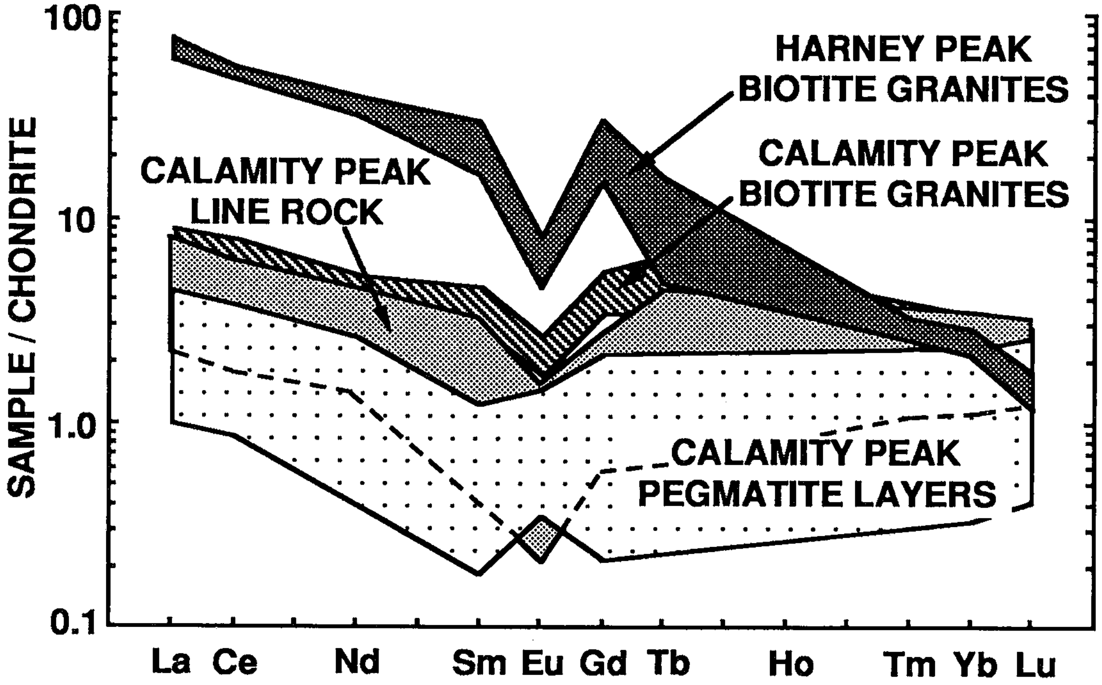

FIG. 7. Composite of chondrite-normalized *REE* patterns showing different rock-types from the Calamity Peak pluton and the range of three Harney Peak biotite granites (unpublished data of C.K. Shearer). Normalized to average chondrite of Haskin *et al.* (1968).

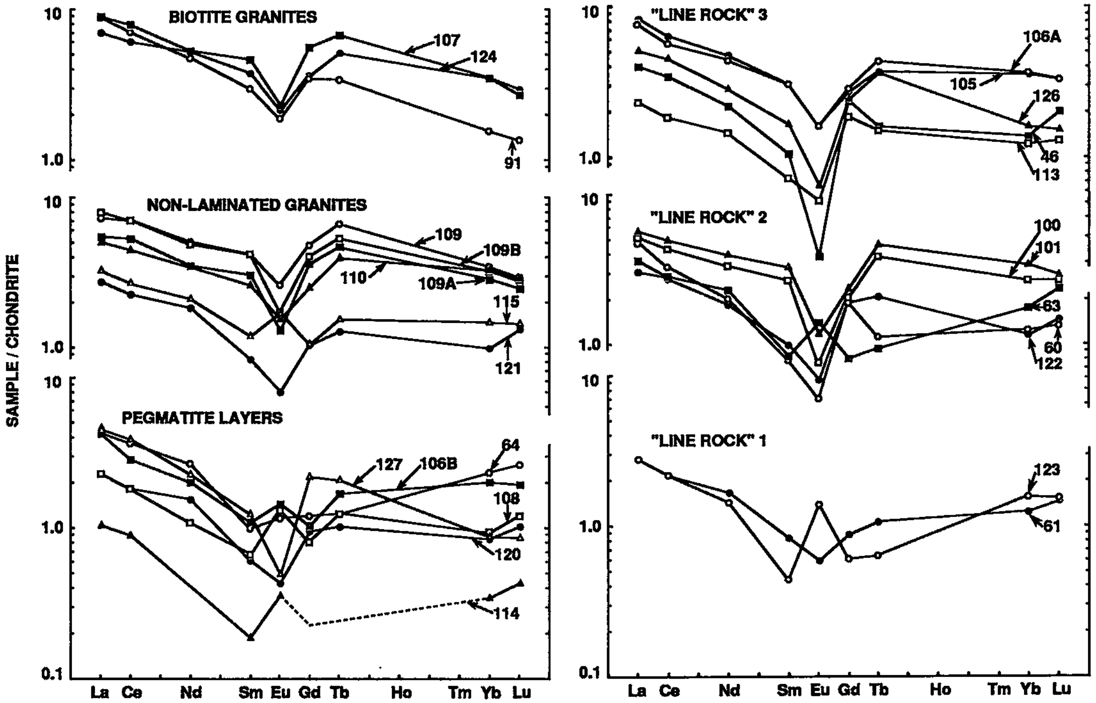

FIG. 8. Individual chondrite-normalized *REE* patterns for samples from the Calamity Peak pluton, arranged by rock type. Note breaks in vertical scale. Data given in Tables 2A and 2B. Values for Ho and Tm not plotted. For clarity, samples of line rock are separated according to their location in the low (1), middle (2), or upper (3) megalayer of Duke *et al.* (1988). Dashed line on pattern for sample 114 shows Gd value based on interpolation from Sm and Yb.

the Calamity Peak area, the granite is generally more heterogeneous and pegmatitic in texture, and displays more fractionated chemical trends of minerals and whole rocks. These are tourmaline-rich granites, with a K/Rb of 200 or much lower. On the basis of the variations in mineral assemblages, mineral chemistry, and whole-rock chemistry, Shearer *et al.* (1987) suggested that the various types of granite in the main dome and surrounding bodies could be related by assuming a Rayleigh fractionation model and 75–80% fractional crystallization of a parent composition similar to certain exposed portions of the central biotite granites. Together with the spatial distribution of the different granite types, with more fractionated bodies toward the perimeter of the dome, the relative age of the different types of granite predicted by this fractional crystallization model agrees with available textural and structural evidence that indicates general outward growth of the entire domal complex (Duke *et al.* 1990).

The fractionation trends in Figure 3 are consistent with those expected from fractional crystallization of the Harney Peak granitic magma. Overall increases in B, Na, P, As, Sb, Lu, and Ta in the Calamity Peak samples, along with decreases in Mg, Ca, Ti, Fe, Sr, Zr, Ba and most *REE*, are typical of fractional crystallization trends in felsic magma series (Miller & Mittlefehldt 1984, Černý & Meintzer 1988, Pichavant *et al.* 1988). The relative enrichment of Na may also reflect phase-equi-

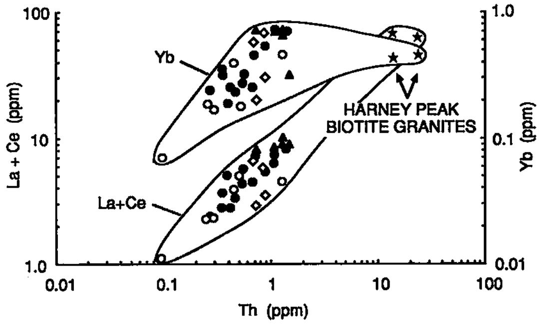

FIG. 9. Plot of whole-rock Th content against La + Ce (left scale) and Yb (right scale) (*cf.* Charoy 1986). Symbols for rock types same as in Fig. 5.

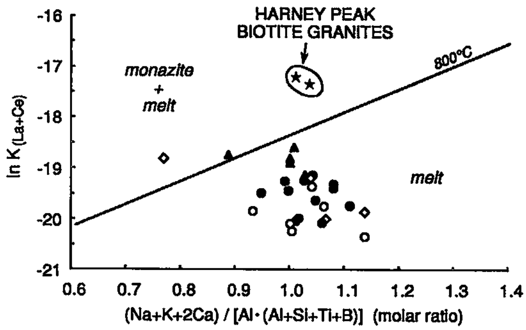

FIG. 10. Experimentally determined limits of saturation of monazite (Montel 1986). Harney Peak biotite granites plot in the monazite-saturated region; most Calamity Peak samples are undersaturated at the conditions of the experiment [800°C, P(H_2O) = 2 kbar]. Value of $\ln K_{(La+Ce)}$ is the molar concentration-product $[La+Ce][PO_4]$. Symbols for rock types same as in Fig. 5.

librium shifts brought about by the high B content of the Calamity Peak magmas, as discussed in a later section. The lack of consistent enrichment of Rb and Cs may reflect the instability of biotite relative to tourmaline in the boron-rich magmas at Calamity Peak; biotite concentrates Rb and Cs by factors of 2.3–2.9 and 11–24, respectively, over K-feldspar, and by factors of 1.7–2.2 and 2.9–3.3, respectively, over muscovite in coexisting mineral separates from Calamity Peak (E.F. Duke, unpubl. data).

Although the samples analyzed in this study span the entire layered sequence, progressive chemical changes with height, analogous to cryptic layering in mafic intrusive bodies, could not be clearly substantiated. In general, Rb correlates positively and Sr negatively with apparent height. Thus K/Rb and Sr/Rb appear to decrease upward and outward in the dome-like pluton; however, the magnitude of the chemical shifts is small, and the correlation coefficients are likewise poor.

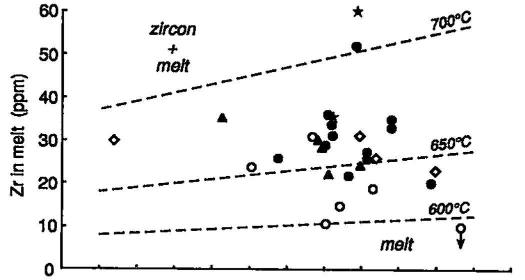

FIG. 11. Experimentally determined limits of saturation of zircon (Watson & Harrison 1983). Temperature and Zr concentrations are extrapolated below range of experiments. Downward arrow indicates value below detection limit. Symbols for rock types same as in Fig. 5.

Behavior of the rare-earth elements

The averages for each rock-type at Calamity Peak show uniform depletion of the *LREE* and Gd, slightly less pronounced depletion of Eu, and *HREE* that range from depleted (Tb) to slightly enriched (Lu) with respect to the less fractionated Harney Peak biotite granites (Figs. 3, 7). These trends suggest that the evolution of the *REE* was controlled by fractionation of one or more *LREE*- to middle-*REE*-rich phases such as monazite, allanite, or apatite, with relatively insignificant control by zircon, xenotime, or garnet (Miller & Mittlefehldt 1982). Apparent greater decreases in Zr than in Hf may, however, indicate some role of zircon in the fractionating assemblage. Zircon, monazite, and apatite are known to occur in the Harney Peak Granite (Redden *et al.* 1982) and at Calamity Peak (Tables 1A, 1B). However, the very strong depletion observed in Th, greater than that for Zr, Y, or U, suggests that the depletion in *LREE* was most closely tied to monazite fractionation (see also Yurimoto *et al.* 1990). These points are illustrated graphically in Figure 9. The near-linear correlation of Th with La + Ce in the Calamity Peak suite and two samples of Harney Peak biotite granite indicates that monazite fractionation controlled *LREE* behavior. The poorer correlation between Th and Yb shows that minerals other than monazite probably controlled the *HREE*, possibly a combination of zircon and garnet.

Accompanying the general depletion in the *REE*, Eu/Eu^* increases in the samples from Calamity Peak relative to the Harney Peak biotite granites, becoming greater than 1 in some samples (Tables 2A, 2B). This suggests that the feldspars may not have been important minerals in the fractionating assemblage; feldspars may have accumulated locally, or $f(O_2)$ may have increased.

Figure 10, based on the work of Montel (1986), emphasizes that melts with the composition of the Harney Peak biotite granites would be oversaturated with respect to monazite, in agreement with its documented occurrence in the some samples of biotite granite (Redden *et al.* 1990). Montel's experimental data are for 800°C; at lower temperatures, monazite saturation is likely to occur at lower concentrations of the *LREE* (lower $\ln K_{La+Ce}$) than those shown in Figure 10 (*cf.* Watson & Harrison 1983, Miller & Mittlefehldt 1982, Rapp *et al.* 1987). This could explain the observation of monazite in several samples from Calamity Peak (Table 1A).

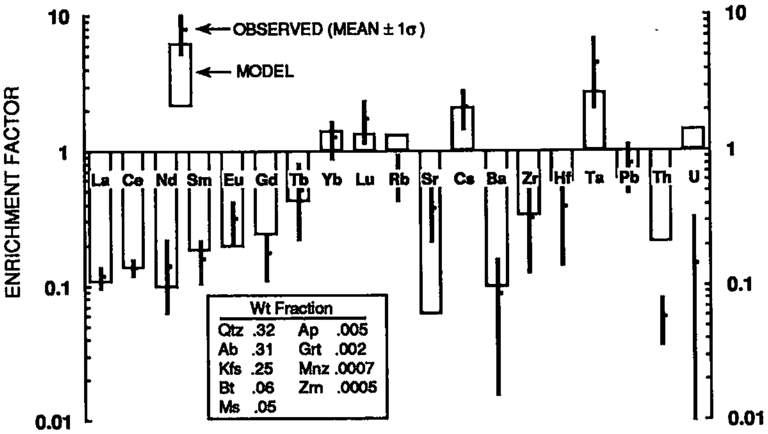

FIG. 12. Comparison of observed enrichment-factors with results of the Rayleigh fractionation model. Enrichment factor defined as the average concentration of seven Calamity Peak biotite granites divided by the average for four Harney Peak biotite granites. Model assumes 70% crystallization of the assemblage shown in the figure. One standard deviation of the mean is calculated by propagating one standard deviation of the average Calamity Peak and Harney Peak values through the calculation of enrichment factors.

Figure 11, based on the findings of Watson & Harrison (1983), indicates that most of the Harney Peak and Calamity Peak compositions also were close to zircon saturation. However, it should be noted that the plotted Zr contents and temperatures are below the lower limit of the original experiments (~ 100 ppm Zr, 750°C). In the case of both Figure 10 and Figure 11, it is apparent that melts with compositions of the pegmatitic layers would be the least likely to reach saturation with either monazite or zircon, unless these crystallized at significantly lower temperatures than the other rock-types.

TABLE 3. MINERAL/MELT DISTRIBUTION COEFFICIENTS USED IN TRACE-ELEMENT MODELING

	Quartz^1	Albite^1	K-feldspar^1	Muscovite^2	Biotite^1	Garnet^3	Zircon^4	Monazite^5	Apatite^3
La	0.014	0.32	0.07	1.28	1.28	0.29*	26.6	3700*	27*
Ce	0.006	0.21	0.04	1.21	1.21	0.35	23.5	3400	34.7
Nd	0.009	0.14	0.03	1.08	1.08	0.53	22	3700	57.1
Sm	0.008	0.11	0.02	1.05	1.05	2.66	17.7	2900	62.8
Eu	0.031	3.8	3.3	0.59	0.59	1.50	12	200	30.4
Gd	0.0073*	0.096*	0.013*	0.93	0.93*	10.5	28.5*	2600	56.3
Tb	0.007	0.09	0.01	0.87	0.87	17.5*	37	1900*	53*
Yb	0.012	0.06	0.03	0.6	0.6	39.9	490	270	23.9
Lu	0.020	0.06	0.04	0.6	0.6	29.6	635	250	20.2
Rb	0.012	0.09	1.6	1.6	4.1	0.0085	—	—	—
Sr	—	6.8	4.7	0.53	0.29	0.015	—	—	2.4^6
Cs	0.022	0.09	0.14	0.65	4.4	—	4.4	—	—
Ba	0.015	0.63	7.2	11	5.6	0.017	—	—	—
Zr	—	0.04	0.01	0.86	0.79	—	3500**	—	—
Hf	0.018	0.06	0.02	0.44	0.44	—	2645	—	—
Ta	0.007	0.02	0.001	1.2	1.2	—	54.8	—	—
Pb	—	1.3	3.2	2.1	1.6	—	—	—	—
Th	0.006	0.03	0.02	0.27	0.27	—	62.4	3000	48^7
U	0.018	0.05	0.04	0.46	0.46	—	298	400	37^8

Sources of data: 1 Nash & Crecraft (1985, sample TP4). 2 Assumed same as biotite for REE, Hf, Ta, Th, U; otherwise calculated from biotite value based on average biotite/muscovite partitioning in Shearer et al. (1986). 3 Arth (1976). 4 Mahood & Hildreth (1983, sample BT(L)). 5 Charoy (1986, calculated from mineral/whole rock data for sample CARN 3); see also discussion in Yurimoto et al. (1990). 6 Watson & Green (1981). 7 Altschuler et al. (1958, calculated from mineral/whole rock data). 8 Calculated assuming Th/U of 1.3 (Hurley & Fairbairn 1955). * Value interpolated or extrapolated from chondrite-normalized pattern. ** Value calculated from mineral/whole-rock data.

Trace-element modeling

A petrogenetic model based on trace-element fractionation is presented to evaluate the observed geochemical variations on a quantitative basis. Included in the model are elements for which precise analytical data are available for most Calamity Peak samples and Harney Peak biotite granites, and for which data on mineral/melt partition coefficients are available between the appropriate minerals and felsic magma.

Results of a model that simultaneously satisfies most of the observed variations in trace element concentrations are shown in Figure 12. Liquid (melt) and solid compositions were calculated using equations for fractional (Rayleigh) crystallization: $C^i_L = C^i_0 F^{(D^i-1)}$, where F is equal to the weight fraction of liquid, C^i_0 is the initial concentration of component *i* in the parent melt, C^i_L is the concentration of component *i* in the melt as crystallization proceeds, and D^i, the bulk solid/melt distribution coefficient for component *i*, is the summation of the individual mineral/melt distribution coefficients multiplied by the weight fractions of the individual minerals.

The Calamity Peak biotite granites are used in the model for two reasons: (1) structural and chemical features indicate that these are the most primary magmas represented in the pluton, and (2) nearly all of the other common rock-types were subject to extensive mineralogical and chemical segregation during crystallization, which has totally obscured the original bulk-composition of those magmas. The model assumes 70% fractional crystallization of a parent melt whose composition is the average of a composite of four Harney Peak biotite granite samples (Tables 1A, 2A). Partition coefficients and sources of information are shown in Table 3. For internal consistency, partition coefficients for most minerals were taken from the data of Nash & Crecraft (1985); these include most minerals of interest, and the SiO_2 content of their melt composition (73.8 wt%) matches closely that of the Harney Peak biotite granite samples. Unfortunately, the study of Nash & Crecraft pertains to a calc–alkaline rhyolite rather than boron-rich peraluminous compositions, and temperatures of mineral/melt equilibration also may have been higher.

The fractionating mineral assemblage shown in Figure 12 is consistent with the normative and modal mineralogy of the biotite granites, except that the zircon and monazite content in the model (about 0.03 and 0.035 vol.%, respectively) appear to be unrealistically high, perhaps by a factor of 5–10, compared with the chemistry and petrography of the Harney Peak biotite granites. Inappropriate choice of (low) partition coefficients for these minerals, or the existence of unsampled zircon- and monazite-enriched cumulate granites, could explain these discrepancies. In the case of monazite, the effective partition-coefficients for Th and *LREE* were derived from a ratio of mineral to whole rock in a granitic rock (see notes, Table 3), and are therefore likely to be low relative to a mineral/glass partition coefficient because of the inability to account for additional monazite in the whole-rock matrix. Furthermore, since Th and *LREE* are stoichiometric components of monazite, the apparent mineral/melt partitioning will increase as the whole-rock *LREE* are depleted to low values, such as occur in the Calamity Peak samples. For example, the ratio of mineral to whole rock increases by a factor of about four between the "most mafic" granite and "most felsic" pegmatite samples, as reported by Mittlefehldt & Miller (1983). The partition coefficient also increases with decreasing temperature or dissolved water in granitic melts (Rapp & Watson 1986).

Figure 12 compares the Calamity Peak biotite granites to the "primitive" Harney Peak biotite granites. The fractional crystallization model predicts the observed enrichment or depletion of many trace elements within one standard deviation of the mean. The slight discrepancy with Eu may reflect $f(O_2)$ effects on Eu^{3+}/Eu^{2+}. The observed variations in Rb, Sr, Th, and U, however, clearly do not fit the model. Partition coefficients for U and Th are poorly known, especially in the case of zircon and monazite. The model behavior of Sr is particularly sensitive to the choice of partition coefficients. If the smaller mineral/melt partition coefficients for plagioclase, K-feldspar, and biotite given in Arth (1976) are used, the model falls within the standard deviation of the observed data. The behavior of Rb is not well understood, and the model fit becomes worse if smaller partition-coefficients are used. A composition of a parent magma with about 50% lower Rb than that chosen here would satisfy the model, and might not be out of the question, considering the heterogeneity of the central Harney Peak granites (Shearer *et al.* 1987). Alternatively, a significant loss of Rb to a mobile hydrothermal fluid could also account for the unexpected depletion (*cf.* Candela 1986). Minor Rb metasomatism has been documented in wall rocks immediately adjacent to the Calamity Peak pluton (E. F. Duke, unpubl. data).

Origin of the granite–pegmatite layering

Jahns & Tuttle (1963) proposed a model for the formation of layered granite–pegmatite intrusive bodies that is consistent with many of our structural and chemical observations in the Calamity Peak pluton. According to the Jahns–Tuttle model, initially homogeneous, volatile-rich granitic magma, with a composition near the haplogranite minimum, was injected to form a tabular intrusive sheet. During subsequent crystallization, the material became segregated into an upper pegmatite layer and lower granite layer. Superposition of a large number of such intrusive sheets, each of which separated into an upper pegmatite layer and lower granite layer, could result in a multiply-layered granite–pegmatite complex such as the Calamity Peak pluton (Orville 1960, Jahns & Tuttle 1963, Duke *et al.* 1988).

Jahns & Tuttle (1963) and later investigators have emphasized that the proposed segregation took place in the presence of crystals, melt, and an exsolved aqueous fluid (Jahns & Burnham 1969, Burnham & Nekvasil 1986, Rockhold *et al.* 1987), although some experimental results suggest that a separate fluid may have been present only during the latest stages of crystallization (London *et al.* 1989). Indeed, many authors have suggested that vertical asymmetry of K and Na in granitic pegmatites is, in part, the result of upward transport of K in the aqueous fluid (*e.g.*, Norton *et al.* 1962, Jahns & Tuttle 1963, Jahns & Burnham 1969). However, experimental evidence that an aqueous fluid could promote the observed chemical fractionation of K and Na by direct transport of elements from the crystallizing granite upward in the magma is equivocal. The majority of the experiments on the partitioning of elements between granitic melts and aqueous solutions (with or without added chloride) indicate that the $K/(K+Na)$ of the solution is always lower than that of the coexisting melt (Holland 1972, Carron & Lagache 1980), making it difficult to effect substantial increases in that ratio through vapor-phase transport. Similarly, Rb, Cs, and Ba are all enriched in the upper, pegmatite layer, but their experimentally determined vapor/melt distribution coefficients are all less than unity (Carron & Lagache 1980). Candela (1986) discussed the difficulty of extracting significant amounts of Rb from a crystal–melt system undergoing vapor-phase exsolution, and Ba and Sr have even stronger affinities for the melt.

In contrast, Burnham & Nekvasil (1986) described experimental results with tourmaline-saturated melts in which K was enriched in the coexisting vapor. If the latter situation is generally applicable in B-bearing melts such as those at Calamity Peak, this seems to provide a possible resolution of the dilemma. Selective vapor-phase redistribution of K (and possibly other geochemically similar elements) upward in the intrusive body would result in complementary Na-rich lower portions and explain much of the vertical asymmetry characteristic of the layered granite–pegmatite intrusions and most zoned pegmatites. On the other hand, vertical asymmetry in the distribution of K and Na occurs also in zoned pegmatites and in layered granite–pegmatite intrusive that are not notably rich in B or tourmaline (Orville 1960). This fact suggests that other volatiles may play the same role as B, or that an entirely different explanation must be sought to explain the vertical asymmetry.

Phase equilibria between crystals and melt in the boron-rich Harney Peak Granite also may be invoked to rationalize the formation of Ab- and Or-rich layers, without explicitly requiring transport of K in the fluid phase. Structural and textural relations indicate that crystallization started at the footwall contact with an albite + quartz ± K-feldspar assemblage (Duke *et al.* 1988). Similarly, crystallization experiments with Harney Peak Granite show that quartz and albite are the first liquidus phases for a range of water contents (Huang & Wyllie 1981). Crystallization proceeded upward with intermittent episodes of tourmaline crystallization, resulting in millimeter-scale laminations in the granite layer. Periods of tourmaline undersaturation or supersaturation characterized by albite + quartz ± K-feldspar crystallization (light laminae) alternate with periods of tourmaline + quartz + K-feldspar + albite crystallization (dark laminae). Rockhold *et al.* (1987) argued that if tourmaline is not stable, B is allowed to build up in the melt, which increases the solubility of H_2O in the melt and shifts the minimum in Q–Ab–Or–H_2O toward Ab (Fig. 5B, Pichavant 1981). With each new dark lamination, tourmaline begins to crystallize, and the minimum shifts away from Ab, since the minimum in tourmaline-saturated experiments is essentially the same as that in the B-free system (Pichavant 1981, Benard *et al.* 1985). The shift of the minimum stabilizes an assemblage richer in K-feldspar and quartz, the melt becomes supersaturated with H_2O, and aqueous fluid exsolves. It is not uncommon for granite layers to contain 20 or more dark laminations, indicating an equal number of repetitions of this cycle of crystallization and fluid exsolution. Because roughly one half of the granite layer (light laminations) crystallized at a minimum or along a cotectic shifted toward Ab, whereas the other half (dark laminations) crystallized near the B-free minimum, the bulk composition of the solid is shifted toward Ab as shown in our results (Fig. 5B). Through the effects of B on the phase relations in the haplogranite system, the bulk granite layer became enriched in Ab, whereas the complementary residual melt forming the pegmatite layer became enriched in Or, although the separation of Na and K may have been enhanced by the presence of a dilute aqueous fluid during much of crystallization.

In summary, phase-equilibrium effects related to the high content of B in the Calamity Peak magmas and direct transport of K in an exsolved aqueous fluid could have operated independently or together to promote vertical segregation into Ab-rich granite layers and Or-rich pegmatite layers. In either case, a high H_2O content and lower viscosity in the upper portion of the magma chamber would result in the relatively rapid growth of large megacrysts of K-feldspar, thereby accentuating existing gradients in activity and causing further upward migration of K, and resulting in highly efficient segregation of K-feldspar and albite, with little effect on quartz distribution.

CONCLUSIONS

Relative to the average Harney Peak biotite granite, the Calamity Peak samples show systematic enrichment or depletion in most elements, irrespective of rock-type. The chemical changes are consistent with derivation of the most primitive of the Calamity Peak magmas by 70% fractional crystallization of melts with the composition of average biotite granites, which is in agreement with the studies of Shearer *et al.* (1987) and Yurimoto *et al.* (1990). The specific process of crystal-liquid fractionation, however, is still poorly understood; Shearer *et al.* (1992) and Nabelek *et al.* (1992a, b) have emphasized that local variations in the processes of partial melting also were instrumental in establishing the spectrum of rock chemistry observed in the Harney Peak Granite suite as a whole.

The most notable chemical difference between the rocks at Calamity Peak and the Harney Peak biotite granites is the increase in B at Calamity Peak by a factor of 5–80; this coincides with the ubiquitous occurrence of tourmaline and well-developed igneous layering throughout the pluton. Along with enrichment in B, the Calamity Peak rocks are enriched in Na relative to K. This observation may be attributed to a combination of effects, one of which is the shift of the haplogranite minimum toward Ab-rich compositions with addition of B (Pichavant 1981). This effect may have been amplified by preferential loss of relatively K-rich melt or vapor phases either to the wall rocks or to the eroded upper portion of the dome-like pluton.

Samples from Calamity Peak display an order-of-magnitude depletion in *LREE* relative to average Harney Peak biotite granite, with the pegmatite layers exhibiting the strongest depletion. The strong correlation between *REE* and Th suggests that monazite stability exerted the dominant control on the evolution of the *REE* from biotite granite such as that of the Harney Peak dome up to and including the different analyzed rock-types in the Calamity Peak pluton.

Fractional crystallization in a portion of the main Harney Peak Granite dome to produce the derivative magmas forming the Calamity Peak pluton agrees with structural evidence constraining the relative timing of growth of the main dome and the Calamity Peak structure (Duke *et al.* 1988). The host rocks of the Calamity Peak pluton were rotated to steep south-southeasterly dips prior to beginning of growth of the Calamity Peak structure. The rotation is attributed to growth of the main Harney Peak Granite dome; thus most of the Harney Peak Granite dome was apparently emplaced prior to development of the Calamity Peak pluton. Extraction of melts from a portion of the main dome to form the Calamity Peak pluton fits the proposed time-constraints based on the structural evolution of the region.

The internal chemical variation in the pluton is dominated by variations between granite-textured and pegmatite-textured layers, which alternate on a scale of 0.1–2.0 m. Sodium, Ca, B, Fe, Mg, Zn, and possibly Mn are partitioned into the granite layers in accordance with their incorporation into albite, tourmaline, and garnet, the characteristic minerals of the granite layers. Potassium, Rb, Cs, Ba, and Pb are partitioned into the pegmatite layers, which are characterized by a relative abundance of perthite. Associated granite and pegmatite layers were derived from a single, homogeneous melt and result from efficient segregation during crystallization into an upper pegmatite layer and lower granite layer. We suggest that through the effects of B and tourmaline crystallization on phase relations in the haplogranite system, the bulk granite layer became enriched in Ab, whereas the complementary residual melt forming the pegmatite layer became enriched in Or.

The separation of Na and K may have been enhanced by the presence of an aqueous fluid during much of crystallization. This fluid, along with some dissolved solutes, migrated upward toward the hanging wall (where it may have become redissolved in the melt) and effected changes in melt composition and melt properties in the magma forming the pegmatitic layer. The fluid would serve to reduce melt viscosity, and thereby increase diffusivities of components, which could aid in the development of the large crystals that characterize the pegmatite layer. The fluid may have enhanced the redistribution of solute by direct transport of K to the upper portion of the intrusive body, although a clear experimental basis for this process is lacking. It is also possible that the fluid served simply as an interconnecting medium for diffusion of components in response to activity gradients established by crystallization of the different assemblages of minerals in the different portions of the layers.

ACKNOWLEDGEMENTS

The authors are indebted to D.C. Gosselin for assistance with analytical work and to J.J. Norton and H. Yurimoto for reviewing an earlier version of the manuscript. We thank D.B. Clarke and J.-M. Montel for perceptive reviews, and R.F. Martin for editorial comments. This research was supported by the U.S. Department of Energy under DOE Grant DE-FG02-88ER13982 (JJP) and DOE Contract DE-AC06-76RLO-1830 (JCL).

REFERENCES

ALTSCHULER, Z.S., JR., CLARKE, R.S. & YOUNG, E.J. (1958): The geochemistry of uranium in apatite and phosphorite. *U.S. Geol. Surv., Prof. Pap.* **314-D**, 45-90.

ARTH, J.G. (1976): Behavior of trace elements during magmatic processes - a summary of theoretical models and their applications. *J. Res. U.S. Geol. Surv.* **4**, 41-47.

BENARD, F., MOUTOU, P. & PICHAVANT, M. (1985): Phase relations of tourmaline leucogranites and the significance of tourmaline in silicic magmas. *J. Geol.* **93**, 271-291.

BURNHAM, C.W. & NEKVASIL, H. (1986): Equilibrium properties of granite pegmatite magmas. *Am. Mineral.* **71**, 239-263.

CANDELA, P.A. (1986): Generalized mathematical models for the fractional evolution of vapor from magmas in terrestrial and planetary crusts. *In* Chemistry and Physics of Terrestrial Planets (S.K. Saxena, ed.). *Adv. Phys. Geochem.* **6**, 362-396.

CARRON, J.-P. & LAGACHE, M. (1980): Étude expérimentale du fractionnement des éléments Rb, Cs, Sr et Ba entre feldspaths alcalins, solutions hydrothermales et liquides silicatés dans le système Q.Ab.Or.H_2O à 2 kbar entre 700 et 800°C. *Bull. Minéral.* **103**, 571-578.

ČERNÝ, P. (1982): Petrogenesis of granitic permatites. *In* Granitic Pegmatites in Science and Industry (P. Černý, ed.). *Mineral. Assoc. Can., Short-Course Handbook* **8**, 405-461.

______ & MEINTZER, R.E. (1988): Fertile granites in the Archean and Proterozoic fields of rare-element pegmatites: crustal environment, geochemistry, and petrogenetic relationships. *In* Recent Advances in the Geology of Granite-Related Mineral Deposits (R.P. Taylor & D.F. Strong, eds.). *Can. Inst. Min. Metall., Spec. Vol.* **39**, 170-207.

CHAROY, B. (1986): The genesis of the Cornubian batholith (south-west England): the example of the Carnmenellis pluton. *J. Petrol.* **27**, 571-604.

DEWITT, E., REDDEN, J.A., WILSON, A.B., BUSCHER, D. & DERSCH, J.S. (1986): Mineral resource potential and geology of the Black Hills National Forest, South Dakota and Wyoming. *U. S. Geol. Surv., Bull.* **1580**.

DUKE, E.F., REDDEN, J.A. & PAPIKE, J.J. (1988): Calamity Peak layered granite-pegmatite complex, Black Hills, South Dakota. 1. Structure and emplacement. *Geol. Soc. Am. Bull.* **100**, 825-840.

______, SHEARER, C.K., REDDEN, J.A. & PAPIKE, J.J. (1990): Proterozoic granite-pegmatite magmatism, Black Hills, South Dakota: structure and geochemical zonation. *In* The Early Proterozoic Trans-Hudson Orogen of North America (J.F. Lewry & M.R. Stauffer, eds.). *Geol. Assoc. Can., Spec. Pap.* **37**, 253-269.

GOSSELIN, D.C., PAPIKE, J.J., ZARTMAN, R.E., PETERMAN, Z.E. & LAUL, J.C. (1988): Archean rocks of the Black Hills, South Dakota: reworked basement from the southern extension of the Trans-Hudson Orogen. *Geol. Soc. Am. Bull.* **100**, 1244-1259.

HASKIN, L.A., HASKIN, M.A., FREY, F.A. & WILDEMAN, T.R. (1968): Relative and absolute terrestrial abundances of the rare earths. *In* Origin and Distribution of the Elements (L.H. Ahrens, ed.). Pergamon Press, New York (889-912).

HOLLAND, H.D. (1972): Granites, solutions and base metal deposits. *Econ. Geol.* **67**, 281-301.

HUANG, W.L. & WYLLIE, P.J. (1981): Phase relationships of S-type granite with H_2O to 35 kbar: muscovite granite from Harney Peak, South Dakota. *J. Geophys. Res.* **86**, 10515-10529.

HURLEY, P.M. & FAIRBAIRN, H.W. (1955): Ratio of thorium to uranium in zircon, sphene, and apatite. *Geol. Soc. Am. Bull.* **66**, 1578 (abstr.).

JAHNS, R.H. & BURNHAM, C.W. (1969): Experimental studies of pegmatite genesis. I. A model for the derivation and crystallization of granitic pegmatites. *Econ. Geol.* **64**, 843-864.

______ & TUTTLE, O.F.(1963): Layered pegmatite-aplite intrusives. *Mineral. Soc. Am., Spec. Pap.* **1**, 78-92.

KRETZ, R. (1983): Symbols for rock-forming minerals. *Am. Mineral.* **68**, 277-279.

LAUL, J.C. (1979): Neutron activation analysis of geological materials. *Atomic Energy Rev.* **17(3)**, 603-695.

LONDON, D. (1990): The berlinite substitution, AlP = 2Si, in alkali feldspars from differentiated peraluminous igneous rocks (granites, pegmatites, and rhyolites). *Geol. Soc. Am., Abstr. Programs* **22**, A346.

______ MORGAN, G.B., VI & HERVIG, R.L. (1989): Vapor-undersaturated experiments with Macusani glass + H_2O at 200 MPa, and the internal differentiation of granitic pegmatites. *Contrib. Mineral. Petrol.* **102**, 1-17.

LUTH, W.C., JAHNS, R.H. & TUTTLE, O.F. (1964): The granite system at pressures of 4 to 10 kilobars. *J. Geophys. Res.* **69**, 759-773.

MAHOOD, G. & HILDRETH, W.E. (1983): Large partition coefficients for elements in high-silica rhyolites. *Geochim. Cosmochim. Acta* **47**, 11-30.

MILLER, C.F. & MITTLEFEHLDT, D.W. (1982): Depletion of light-rare earth elements in felsic magmas. *Geology* **10**, 129-133.

______ & ______ (1984): Extreme fractionation in felsic magma chambers: a product of liquid-state diffusion or fractional crystallization? *Earth Planet. Sci. Lett.* **68**, 151-158.

MITTLEFEHLDT, D.W. & MILLER, C.F. (1983): Geochemistry of the Sweetwater Wash pluton, California: implications for "anomalous" trace element behavior during differentiation of felsic magmas. *Geochim. Cosmochim. Acta* **47**, 109-124.

MONTEL, J.-M. (1986): Experimental determination of the solubility of Ce-monazite in SiO_2-Al_2O_3-K_2O-Na_2O melts at 800°C, 2 kbar, under H_2O-saturated conditions. *Geology* **14**, 659-662.

NABELEK, P.I., RUSS-NABELEK, C. & DENISON, J. (1992a): The generation and crystallization conditions of the Proterozoic Harney Peak leucogranite, Black Hills, South Dakota, USA: petrologic and geochemical constraints. *Contrib. Mineral. Petrol.* **110**, 173-191.

______, ______ & HAEUSSLER, G.T. (1992b): Stable isotope evidence for the petrogenesis and fluid evolution in the Proterozoic Harney Peak leucogranite, Black Hills, South Dakota. *Geochim. Cosmochim. Acta* **56**, 403-417.

NASH, W.P. & CRECRAFT, H.R. (1985): Partition coefficients for trace elements in silicic magmas. *Geochim. Cosmochim. Acta* **49**, 2309-2322.

NORTON, J.J., PAGE, L.R. & BROBST, D.A. (1962): Geology of the Hugo pegmatite, Keystone, South Dakota. *U.S. Geol. Surv., Prof. Pap.* **297-B**, 49-127.

______ & REDDEN, J.A. (1990): Relations of zoned pegmatites to other pegmatites, granite, and metamorphic rocks in the southern Black Hills, South Dakota. *Am. Mineral.* **75**, 631-655.

______ *et al.* (1964): Geology and mineral deposits of some pegmatites in the southern Black Hills, South Dakota. *U.S. Geol. Surv., Prof. Pap.* **297-E**, 293-341.

ORVILLE, P.M. (1960): Petrology of several pegmatites in the Keystone district, Black Hills, South Dakota. *Geol. Soc. Am. Bull.* **71**, 1467-1490.

PAGE, L.R. *et al.* (1953): Pegmatite investigations, 1942-1945, Black Hills, South Dakota. *U. S. Geol. Surv., Prof. Pap.* **247**.

PICHAVANT, M. (1981): An experimental study of the effect of boron on a water saturated haplogranite at 1 kbar vapor pressure. Geological applications. *Contrib. Mineral. Petrol.* **76**, 430-439.

______, KONTAK, D.J., BRIQUEU, L., HERRERA, V.J. & CLARK, A.H. (1988): The Miocene–Pliocene Macusani volcanics, southeast Peru. II. Geochemistry and origin of felsic peraluminous magma. *Contrib. Mineral. Petrol.* **100**, 325-338.

RAPP, R.P., RYERSON, F.J. & MILLER, C.F. (1987): Experimental evidence bearing on the stability of monazite during crustal anatexis. *Geophys. Res. Lett.* **14**, 307-310.

______ & WATSON, E.B. (1986): Monazite solubility and dissolution kinetics: implications for the thorium and light rare earth chemistry of felsic magmas. *Contrib. Mineral. Petrol.* **94**, 304-316.

REDDEN, J.A. (1963): Geology and pegmatites of the Fourmile quandrangle, Black Hills, South Dakota. *U. S. Geol. Surv., Prof. Pap.* **297-D**, 199-291.

______, NORTON, J.J. & MCLAUGHLIN, R.J. (1982): Geology of the Harney Peak Granite, Black Hills, South Dakota. *U.S. Geol. Surv., Open-File Rep.* **82-481**.

______, PETERMAN, Z.E., ZARTMAN, R.E. & DEWITT, E. (1990): U–Th–Pb geochronology and preliminary interpretation of Precambrian tectonic events in the Black Hills, South Dakota. *In* The Early Proterozoic Trans-Hudson Orogen of North America (J.F. Lewry & M.R. Stauffer, eds.). *Geol. Assoc. Can., Spec. Pap.* **37**, 229-251.

RILEY, G.H. (1970): Isotopic discrepancies in zoned pegmatites, Black Hills, South Dakota. *Geochim. Cosmochim. Acta* **34**, 713-725.

ROCKHOLD, J.R., NABELEK, P.I. & GLASCOCK, M.D. (1987): Origin of rhythmic layering in the Calamity Peak satellite pluton of the Harney Peak Granite, South Dakota: the role of boron. *Geochim. Cosmochim. Acta* **51**, 487-496.

SCHALLER, W.T. (1925): The genesis of lithium pegmatites. *Am. J. Sci.* **210**, 269-279.

SHANNON, J.R., WALKER, B.M., CARTEN, R.B. &

GERACHTY, E.P. (1982): Unidirectional solidification textures and their significance in determining relative ages of intrusions at the Henderson mine, Colorado. *Geology* **10**, 293-297.

SHEARER, C.K., PAPIKE, J.J. & JOLLIFF, B.L. (1992): Mineralogical and chemical evolution of the Harney Peak rare element granite - pegmatite system, Black Hills, South Dakota: petrogenetic links between granites and pegmatites. *Can. Mineral.* **30**,

______, ______ & LAUL, J.C. (1987): Mineralogical and chemical evolution of a rare-element granite-pegmatite system: Harney Peak Granite, Black Hills, South Dakota. *Geochim. Cosmochim. Acta* **51**, 473-486.

______, ______, SIMON, S.B. & LAUL, J.C. (1986): Pegmatite–wallrock interactions, Black Hills, South Dakota: interaction between pegmatite-derived fluids and quartz–mica schist wallrock. *Am. Mineral.* **71**, 518-539.

WALKER, R.J., HANSON, G.N., PAPIKE, J.J. & O'NEIL, J.R. (1986): Nd, O and Sr isotopic constraints on the origin of Precambrian rocks, southern Black Hills, South Dakota. *Geochim. Cosmochim. Acta* **50**, 2833-2846.

WATSON, E.B. & GREEN, T.H. (1981): Apatite/liquid partition coefficients for the rare earth elements and strontium. *Earth Planet. Sci. Lett.* **56**, 405-421.

______ & HARRISON, T.M. (1983): Zircon saturation revisited: temperature and composition effects in a variety of crustal magma types. *Earth Planet. Sci. Lett.* **64**, 295-304.

YURIMOTO, H., DUKE, E.F., PAPIKE, J.J. & SHEARER, C.K. (1990): Are discontinuous chondrite-normalized *REE* patterns in pegmatitic granite systems the result of monazite fractionation? *Geochim. Cosmochim. Acta* **54**, 2141-2145.

Received October 1, 1990, revised manuscript accepted November 15, 1991.